Geological Quarterly, 2022, 66: 20
DOI: http://dx.doi.org/10.7306/gq.1652

The Silesian Ridge in the light of petrological and LA-ICP-MS U-Pb analyses of cohesive debrites from the Istebna Formation (Silesian Nappe, Outer Western Carpathians, Poland)

Monika SZCZUKA[1, *], Aleksandra GAWĘDA[2], Anna WAŚKOWSKA[1], Jan GOLONKA[1], Krzysztof SZOPA[2], David CHEW[3] and Foteini DRAKOU[3]

[1] AGH University of Science and Technology in Kraków, Faculty of Geology, Geophysics and Environmental Protection, Al. A. Mickiewicza 30, 30-059 Kraków, Poland

[2] University of Silesia in Katowice, Faculty of Natural Sciences, Institute of Earth Sciences, Będzińska 60, 41-200 Sosnowiec, Poland

[3] Trinity College Dublin, Department of Geology, School of Natural Sciences, Dublin 2, Ireland

Szczuka, M., Gawęda, A., Waśkowska, A., Golonka, J., Szopa, K., Chew, D., Drakou, F., 2022. The Silesian Ridge in the light of petrological and LA-ICP-MS U-Pb analyses of cohesive debrites from the Istebna Formation (Silesian Nappe, Outer Western Carpathians, Poland). Geological Quarterly, 2022, 66: 16, doi: 10.7306/gq.1648

Exotic clasts present in flysch deposits of the Western Outer Carpathians enable investigation and reconstruction of the eroded crystalline basement of the Silesian Ridge. The flysch rocks of the Istebna Formation (Jasnowice Member: Paleocene) in the Silesian Nappe contain magmatic and metamorphic clasts derived from the Silesian Ridge basement. The crystalline rock fragments acquired from cohesive debrites were analyzed petrographically and geochemically, and zircon and rutile crystals were subject to LA-ICP-MS U-Pb dating. Granitoid clasts yielded Meso-Variscan U-Pb zircon ages (325.7 and 330.6 Ma), with older (Neoproterozoic to Paleoproterozoic) inherited cores and εNd_{330} = –12.0 (TDM age of 1.98 Ga). The orthogneiss clast yielded a protolith age of 1635 Ma and fingerprint of thermal reworking at ~288 Ma. Zircon crystals from the detrital clasts yielded similar U-Pb zircon ages to the granitoid clasts (311.5 to 391 and 331 Ma). The rutile crystals from sandstone yielded concordia age of 344.7 Ma. Zircon crystals from paragneiss, interpreted as a granitoid envelope, yielded $^{238}U/^{206}Pb$ ages between 557 and 686 Ma and include an inherited core of age ~1207.4 ±33.8 Ma. Age data from exotic clasts and the detrital zircon and rutile fraction suggest the core part of the Silesian Ridge was a Neoproterozoic to Mesoproterozoic envelope intruded by Meso-Variscan granitoid plutons.

Key words: Outer Carpathians, Silesian Ridge, exotic clasts, U-Pb dating, zircon, rutile.

INTRODUCTION

The Carpathians are one of the largest mountain ranges in Europe, extending for over 1,300 km (Fig. 1A; Golonka et al., 2021a). They formed as a result of the Cretaceous to Neogene collision of several microplates with the European Platform (e.g., Golonka and Picha, 2006; Gawęda and Golonka, 2011). The Western Carpathians are traditionally divided into the internal Central Carpathians and the external Outer Carpathians, separated by the narrow Pieniny Klippen Belt (e.g., Oszczypko, 2004, 2006). The Outer Carpathians nappes are mainly composed of sedimentary rocks of flysch character (Fig. 1B) (Golonka et al., 2005, 2021a; Ślączka et al., 2006), that were deposited on crystalline basement within the Tethys Ocean. However the nature and origin of this crystalline basement is poorly understood as it was present only in uplifted ridges, subjected to strong erosion. Characterizing the nature of the crystalline basement of the ridges is restricted to investigating exotic blocks that represent eroded basement portions, redeposited by density currents (e.g., Budzyń et al., 2011; Gawęda et al., 2019a; Burda et al., 2019). The blocks were derived from elevated basement blocks (ridges) that are characteristic of the outermost Tethys (Golonka et al., 2019). One of these ridges, the Silesian Ridge, was a key structure in Mesozoic and Cenozoic palaeogeography. It was a long-lived basement high, separating the Magura Basin in the south from the Silesian Basin in the north (Fig. 2; e.g., Unrug, 1968; Książkiewicz, 1975; Eliáš et al., 2003; Golonka et al., 2006, 2019). The NW–SE trending Silesian Ridge was part of the European Platform within the western part of the Outer Carpathian basins. The Silesian Ridge was present from Jurassic to Neogene times. Its development was multistage but the western part of the ridge was particularly prominent during the Late Cretaceous to Early Paleocene (Unrug, 1968; Golonka et al., 2003) when it was subject to enhanced erosion.

The resulting clastic material was transported into adjacent basins by gravity flows (Unrug, 1963, 1968; Książkiewicz,

* Corresponding author, e-mail: szczuka@agh.edu.pl

Received: March 9, 2022; accepted: June 27, 2022; first published online: September 6, 2022.

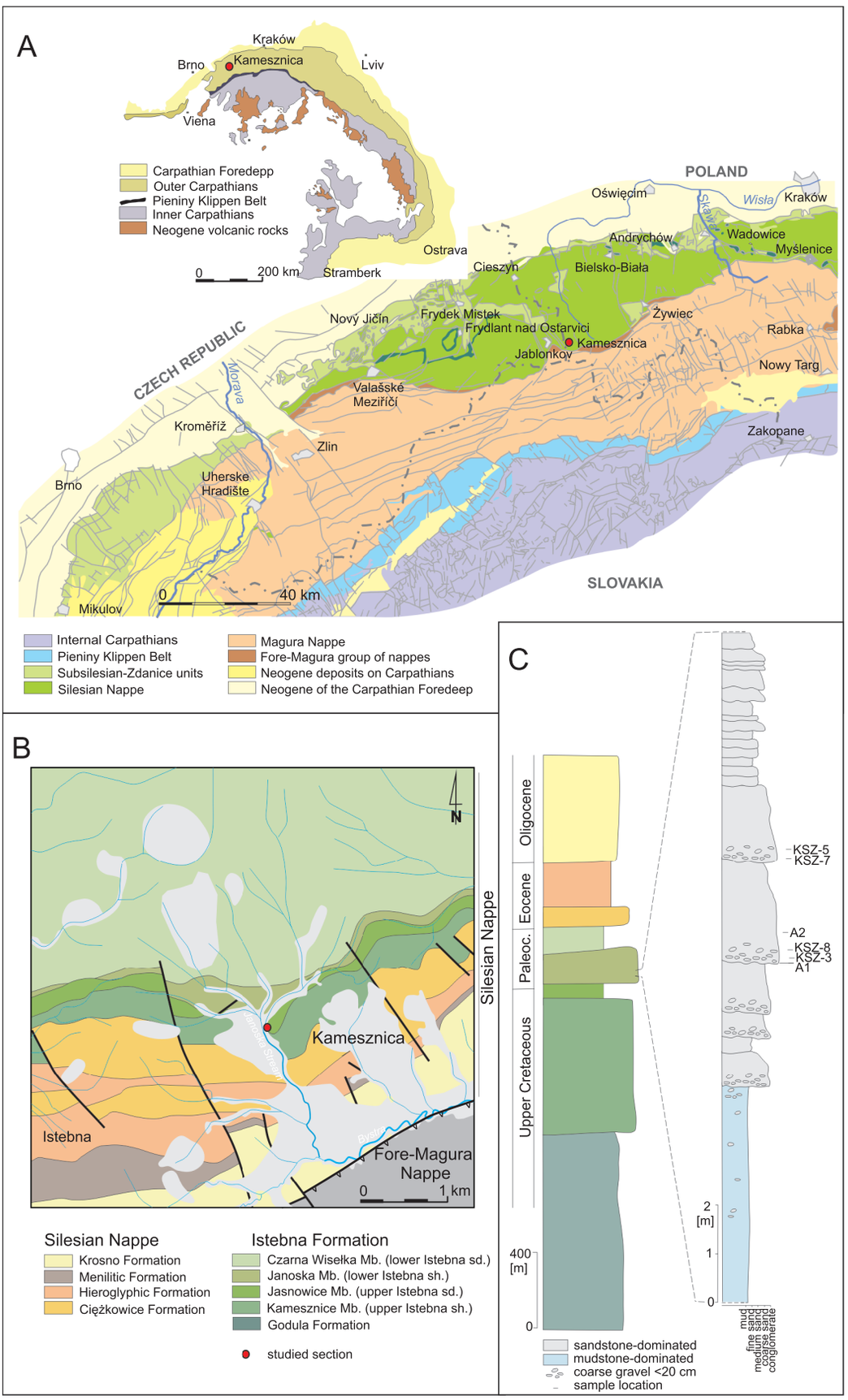

Fig. 1. Location of the study area on (A) a simplified geological map of the Carpathian chain within Europe and the western part of the Carpathians, (B) a detailed geological map of the Silesian Nappe in the area of Kamesznica (based on Burtan et al., 2016 and Ryłko, 2019), and (C) lithostratigraphic section of the Istebna Formation and the analyzed profile

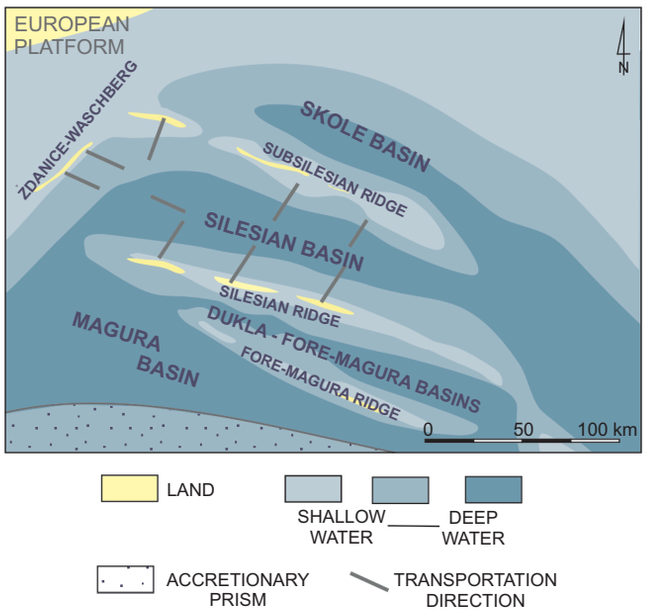

Fig. 2. Palaeotransport directions in the Silesian Basin in the Late Cretaceous–Paleocene (palaeogeographic sketch after Książkiewicz, 1962 and Golonka et al., 2019 – modified)

1975). Basement-derived material is common in the Outer Carpathian deposits, and mainly occurs in the form of detritus in sandstones and finer grained clastic rocks. Larger clasts, which are more useful for characterizing the basement, are not so frequent (e.g., Gaweda et al., 2019a), but are components of olistostromes and debrites of the Istebna Formation of the Silesian Nappe.

This paper reconstructs the lithological character and age of the crystalline basement of the Silesian Ridge, which was the main source of the clastic material in the western part of the Silesian Basin. It includes U-Pb zircon and rutile dating of clasts of crystalline rocks (olistoliths) and U-Pb zircon detrital zircon and rutile dating of the olistostrome matrix as well as of associated sandstones.

GEOLOGICAL BACKGROUND

This study has focused on the Istebna Formation in the Istebna-Milówka area (Silesia Beskidy Mts.) located in western part of the Silesian Nappe in the Outer Carpathians (Fig. 1A). The Istebna Formation was deposited during a phase of pronounced erosion of the Silesian Ridge (Unrug, 1963, 1968; Książkiewicz, 1977). It consists of two thick-bedded sandy and sandy-conglomeratic units: the Czarna Wisełka Member (Campanian-Maastrichtian) and the Jasnowice Member (Paleocene) which are separated by and overlain by shale-dominated successions: the Janoska Member (Maastrichtian–lowermost Paleocene) and the Kamesznica Member (Paleocene) of total thickness of 1800 m (Golonka et al., 2013; Starzec et al., 2017; age after e.g., Geroch, 1960; Fig. 1C). The thick-bedded sandy and sandy-conglomeratic units were formed by gravity flows, and include different types of debrite. They usually contain pebbles, cobbles and boulders of igneous and metamorphic rocks eroded from upper parts of the ridge. These deposits are common in the Jasnowice Member (Strzeboński, 2015) and the cohesive debrites likely represent enhanced pulses of sedimentation from a point source (Cieszkowski et al., 2012 and references therein).

SAMPLING

The sample locality is situated in the marginal, southernmost zone of the Silesian Nappe, close to the Fore-Magura and Magura thrusts (Fig. 1A, B). Samples were taken from the Jasnowice Member (Fig. 1C) that reaches a maximum thickness of ~150 m in this area (Unrug, 1963, 1968). The sampled succession comprised thick- and very thick-bedded sandy conglomerate, gravelly sandstone and conglomerate (Strzeboński, 2015) with a wide spectrum of rock types (Fig. 1C). The sampled section is located in the northern part of Kamesznica Village; studied material was taken from the natural exposures in the Janoska stream bed (GPS: N 49°34'37.8" E 19°00'33.6") (Fig. 1B). The locality consists of a 6.5 m thick succession with six sandy conglomerate cohesive debrite layers underlain by medium-bedded medium- and fine-grained sandstone (Fig. 1C). The sampled section passes upwards into a sequence of medium-bedded turbiditic sandstones (Fig. 1C).

Exotic debrite-type deposits (*sensu* Strzeboński, 2005) occur in the lower parts of the sandy-conglomerate debrite layers (Fig. 1C). The size of the exotic clasts is clearly bigger than those of the host conglomerates (Fig. 3A). They are 10–100 cm across and consist of sandstones, limestones, gneisses, schists and quartzites, as well as granitoids. Six samples were taken from this section: four exotic boulders from the sandy-conglomerate debrites and two samples from clastic deposits (Fig. 1C). Exotic boulders came from the lower parts of two successive thick beds. Clasts KSZ-5, KSZ-7, KSZ-8 with a diameter of ~20–25 cm and clast A-1 of diameter 50 cm were collected for the study. Samples KSZ-3 and A-1 came from the sandy-conglomeratic deposits. Sample KSZ-3 was taken from medium- to fine-grained poorly sorted sandstones of the lowermost part of the layer. Sample A-2 (Fig. 1C) was taken from fine-grained sandstone occurring above the debris conglomerate (Fig. 1C).

ANALYTICAL TECHNIQUES

MICROSCOPY

Thin section petrography was carried out at the Faculty of Natural Sciences of the University of Silesia in Katowice, Poland, using an *Olympus BX-51* microscope to constrain textural and microstructural relationships and to determine the presence of zircon. Petrographic observations were used to select representative samples for subsequent electron probe microanalysis and whole-rock geochemical analyses.

WHOLE-ROCK CHEMICAL AND ISOTOPE ANALYSES

Whole-rock analyses were undertaken by X-ray fluorescence (XRF) for major- and large-ion lithophile trace elements (LILE), and by fusion and ICP-MS for high-field strength elements (HFSE) and rare earth elements (REE) at Bureau Veritas Minerals (Canada). The preparation involved lithium borate fusion and dilute digestions for XRF and lithium borate decomposition or aqua regia digestion for ICP-MS. LOI (lost of ignition) was determined at 1000°C. Uncertainties for most of the major elements are 0.01%, except for SiO_2, which is 0.1%. REEs were normalized to C1 chondrite (McDonough and Sun, 1995).

The Sm-Nd analytical work was performed in the Laboratory of Geochronology, Department of Lithospheric Research, University of Vienna. Results are based on ID-TIMS proce-

Fig. 3. Photographs of the exotic blocks from the Janoska Stream

A – A-1 orthogneiss exotic block, *in situ* (exposure in the Janoska Stream); **B** – microtexture of the matrix of the conglomerate KSZ-3, containing A-1 gneiss; **C** – microtexture of the granitoid KSZ-8; **D** – photomicrograph showing the porphyroblastic paragneiss KSZ-7; **E** – microtexture of the granitoid KSZ-5; Qtz – quartz, Kfs – K-feldspar, Fs – feldspar, Pl – plagioclase, Bt – biotite, Ms – muscovite, Py – pyrite, Rt – rutile, Cc – calcite

dures. Sample digestion for Nd-Sr analysis was performed in *Savillex*® beakers using an ultrapure 4:1 mixture of HF and HNO_3 for 10 days at 110°C on a hot plate. For whole-rock powders, a minimum dissolution time of three weeks was applied to ensure maximum leaching of REEs from refractory material such as zircon. After evaporating the acids, repeated treatment of the residue using HNO_3 and 6.0 N HCl resulted in clear solutions for all samples. The REE fraction was extracted using *AG® 50W-X8* (200-400 mesh, Bio-Rad) resin and 4.0 N HCl. Nd was separated from the REE fraction using teflon-coated *HdEHP* and 0.22 N HCl as the elution medium. The maximum total procedural blanks, 50 pg for Nd, were taken as negligible. Nd was run as metal on a Re double filament, using a *ThermoFinnigan® Triton MC TIMS*. A $^{143}Nd/^{144}Nd$ ratio of 0.511841 ±0.000005 (n = 5) was determined for the international La Jolla (Nd) standard, during the investigation period. The within-run mass fractionation for Nd isotope compositions (IC) was corrected to $^{146}Nd/^{144}Nd = 0.7219$. The uncertainty in the Nd isotope ratio is typically quoted as 2σ.

MINERAL SEPARATION AND IMAGING

Zircon and rutile crystals were separated using standard density separation techniques (crushing, sieving, washing in heavy liquids, and panning). This separation was carried out at the Institute of Geological Sciences of the Polish Academy of Sciences, Kraków, Poland. Zircon and rutile crystals were

handpicked under a binocular microscope, cast in 25 mm diameter epoxy resin mounts, and then ground and polished to expose the grain interiors. Mineral textures were then imaged using back-scattered electron (BSE) and cathodoluminescence (CL) detectors on a *FET Philips 30* scanning electron microscope with a 15 kV accelerating voltage and a beam current of 1 nA at the Faculty of Natural Sciences, University of Silesia in Katowice, Poland.

4LA-ICP-MS U-Pb ZIRCON DATING

LA-ICP-MS U-Pb age data were acquired using a *Photon Machines Analyte Excite 193 nm ArF* excimer laser-ablation system with a *HelEx* 2-volume ablation cell coupled to an *Agilent 7900 ICPMS* at the Department of Geology, Trinity College Dublin. The instrument was tuned using NIST612 standard glass to yield Th/U ratios of unity and low oxide production rates (ThO^+/Th^+ typically <0.15%). A repetition rate of 12 Hz and a circular spot of 24 μm were used. A quantity of 0.4 l min^{-1} He carrier gas was fed into the laser cell, and the aerosol was subsequently mixed with 0.6 l min^{-1} Ar make-up gas and 11 ml min^{-1} N_2. Eight isotopes (^{90}Zr, ^{202}Hg, ^{204}Pb, ^{206}Pb, ^{207}Pb, ^{208}Pb, ^{232}Th and ^{238}U) were acquired during each analysis, which comprised 25 s of ablation and 12 second washout, the latter portions of which were used for the baseline measurement. Data reduction of raw U-Pb isotope data was performed using the "VizualAge" data reduction scheme (Petrus and Kamber, 2012) in the freeware *IOLITE* package (Paton et al., 2011). Sample-standard bracketing was applied after correction of downhole fractionation to account for long-term drift in isotopic or elemental ratios by normalizing all ratios to those of the U-Pb reference standards. Final age calculations were made using the *Excel Isoplot* add-in (Ludwig, 2012). In Appendixes 1–3, the data are quoted with 2σ analytical uncertainties and weighted mean calculations and discordia intercept ages are quoted at the 2σ level and include the decay constant uncertainty. Data with absolute discordance >5% were excluded from age calculations. 91500 zircon ($^{206}Pb/^{238}U$ TIMS age of 1065.4 ±0.6 Ma; Wiedenbeck et al., 1995, 2004) was used as the primary U-Pb calibration standard. The secondary standards AusZ2 zircon ($^{206}Pb/^{238}U$ TIMS age of 38.8963 ±0.0044; Kennedy et al., 2014), Plešovice zircon ($^{206}Pb/^{238}U$ TIMS age of 337.13 ±0.37 Ma; Sláma et al., 2008) and WRS 1348 zircon ($^{206}Pb/^{238}U$ TIMS age of 526.26 ±0.70; Pointon et al., 2012) yielded LA-ICP-MS U-Pb Concordia ages of 39.07 ±0.44 Ma, 340.5 ±1.5 Ma and 525.4 ±2.3 Ma respectively.

LA-ICP-MS U-Pb RUTILE DATING

For the analyses of the rutile crystal ages, the same device was used as for zircon crystal analyses. All data reduction was performed offline using the *IOLITE* data reduction package using the *Vizual Age_UcomPbine* data reduction scheme (Chew et al., 2014). R10 was employed as the primary standard, and R19 (ID-TIMS date of 489.5 ±0.9 Ma; Zack et al., 2011) and R13 (U-Pb SHRIMP age of 504 ±4 Ma, Schmitt and Zack, 2012) were employed as secondary standards and treated as unknowns during data reduction, and yielded weighted average ^{207}Pb- corrected ages of 488.7 ±7.9 Ma and 500.2 ±3.7 Ma respectively. Ages were calculated using the *Isoplot* plug-in for *Excel* (Ludwig, 2012). Common (non-radiogenic) Pb in the primary and secondary standards was corrected with a ^{207}Pb-based correction method using a known initial $^{207}Pb/^{206}Pb$ ratio; common Pb in the unknowns was corrected using an initial estimate of the $^{207}Pb/^{206}Pb$ ratio generated using the terrestrial Pb evolution model of Stacey and Kramers (1975) employing an iterative approach (Bracciali et al., 2013; Chew et al., 2014). Due to the use of the ^{207}Pb-based correction, rutile U-Pb analyses could not be conventionally assessed for discordance, but sometimes the high common Pb to radiogenic Pb ratios resulted in undesirably large age uncertainties. Grains with large age uncertainties were therefore filtered (Mark et al., 2016; O'Sullivan et al., 2016) using the approach of Chew et al. (2020).

RESULTS

PETROGRAPHY AND GEOCHEMISTRY

An exotic block of orthogneiss (A-1) (Fig. 3A, C) is composed of quartz, biotite, plagioclase and K-feldspar and the accessory components are fluorapatite, zircon and Ce-monazite. The sample has 81 wt.% SiO_2 and 10 wt.% Al_2O_3, is peraluminous (ASI = 1.13), with $Na_2O > K_2O$ and Rb/Sr = 0.39 (Table 1). The geochemistry of the A-1 orthogneiss sample is likely modified due to secondary quartz remobilization and crystallization along the foliation planes. The trace element characteristics imply a trachyandesite magmatic protolith (Fig. 4D) after Winchester and Floyd (1977). The sum of REE is 235 ppm, while the chondrite-normalized REE patterns revealed a pronounced negative Eu anomaly of 0.58 and weak REE fractionation (Ce_N/Yb_N = 6.26; Table 1).

Sample KSZ-3 represents the matrix of the conglomerate that contains the A-1 orthogneiss clast. The matrix is medium grained, while sporadically larger (3 to 15 mm in size) clasts are present, cemented by calcite. Clasts of all sizes are poorly rounded and comprise quartz, feldspar, biotite, muscovite, glauconite and accessory minerals such as pyrite, zircon and rutile (Fig. 3B). The mineralogy of the matrix is similar to that of the larger clasts. The sample includes SiO_2 (64 wt.%), CaO (12 wt.%) and Al_2O_3 (7 wt.%) (Table 1).

The sample (A-2) was taken from a fine-grained sandstone overlying a sandy-conglomerate cohesive debrite layer (Fig. 1C). The majority of clasts are composed of quartz and feldspar with a small amount of biotite and muscovite, and are cemented by calcite. The occasionally contains larger grains (3 to 10 mm) that are poorly rounded. Zircon was the only accessory mineral observed. The mineralogy of the matrix is similar to that of the larger clasts. The sample includes SiO_2 (67 wt.%.), CaO (11 wt.%) and Al_2O_3 (7 wt.%) (Table 1).

Sample KSZ-8 is a massive, grey coarse-grained granitoid. It is composed of quartz, chloritized plagioclase, zoned and perthitized K-feldspar, biotite locally replaced by chlorite and zones of deformed muscovite (Fig. 3C). Accessory minerals are mainly zircon (up to 200 μm in size). It is rich in in SiO_2 (Fig. 4A), peraluminous (ASI = 1.23), with $Na_2O > K_2O$ and the Rb/Sr ratio is low (0.19; Table 1). Chondrite-normalized (Sun and McDonough, 1989) and C1-normalized REE patterns show moderate LREE enrichment (Ce_N/Yb_N = 19.84) and a slightly positive Eu anomaly (Eu/Eu* =1.01; Table 1 and Fig. 5A). The whole-rock isotope data of KSZ-8 sample reveals a $^{147}Sm/^{144}Nd$ ratio of 0.089171 ±2 and $^{143}Nd/^{144}Nd$ ratio of 0.511791 ±2. The resulting ΣNd_{330} is – 12.0 (Table 2).

Sample KSZ-7 is a dark grey, porphyroblastic paragneiss (Fig. 3D). The main mineral components are quartz, plagioclase, biotite (commonly in bands and strongly deformed) and muscovite, with the micas defining the foliation in the sample. The sample is also veined by calcite concordant with the folia-

Table 1

Chemical composition and selected petrological indices of the whole-rock samples of rocks from the Janoska Stream

Sample no.	A-1	KSZ-3	A-2	KSZ-5	KSZ-7	KSZ-8
SiO_2	80.50	63.62	66.60	70.01	71.24	74.72
TiO_2	0.26	0.01	0.14	0.16	0.40	0.10
Al_2O_3	10.00	7.04	6.54	15.77	14.66	15.01
Fe_2O_3	2.35	1.90	1.09	0.58	2.85	1.00
MnO	0.03	0.12	0.08	0.01	0.02	0.01
MgO	0.28	1.01	0.44	0.13	1.43	0.30
CaO	1.16	11.70	11.40	1.49	1.21	0.48
Na_2O	2.53	1.37	1.27	3.61	4.56	5.56
K_2O	2.49	2.41	2.56	7.28	1.99	2.20
P_2O_5	0.05	0.05	0.03	0.21	0.11	0.07
LOI	0.52	10.64	9.60	1.19	1.88	0.84
Total	100.17	99.87	99.75	100.44	100.35	100.29
ppm						
Sr	108.7	202.3	197.1	143	145.2	302.4
Ba	1145	539	584	945	337	611
Rb	42.2	73.6	74.3	198.3	58.9	56.8
Th	10.9	7	4.4	5.1	17.9	3.9
U	3.1	3	1.1	2.6	2.5	0.6
Ni	3.5	9.2	5.6	5.2	2.9	4.7
Pb	11.3	5.5	6.8	7	2.4	3.1
Co	12.4	3.3	4.3	11.9	3.8	20.6
Ga	12.5	6.1	5.5	12.8	18.4	13.1
V	<8	18	10	<8	23	<8
Zr	279	116.4	82.2	72.6	186.5	70.1
Hf	8	3.1	2.3	2.3	5	2
Y	34.7	11.1	9.7	19.3	11	4.1
Nb	16.1	3.9	2.5	6.5	12.6	4.6
Ta	1	0.3	0.3	1.1	1.1	0.2
La	46.9	16.4	12.5	14.9	69.6	19.9
Ce	96.1	32.1	22.6	26.1	124.6	28.7
Pr	10.95	3.52	2.57	3.08	14.16	3
Nd	43	13.2	10.1	11	49.4	10.1
Sm	8.45	2.42	1.8	2.39	6.99	1.49
Eu	1.58	0.53	0.52	1.06	1	0.43
Gd	8.05	2.16	1.76	2.65	4.37	1.13
Tb	1.26	0.34	0.24	0.51	0.48	0.15
Dy	7.79	2.08	1.56	3.25	2.32	0.86
Ho	1.4	0.41	0.33	0.67	0.38	0.14
Er	4.49	1.27	0.91	2.12	0.96	0.42
Tm	0.58	0.18	0.12	0.33	0.13	0.05
Yb	4.03	1.10	0.82	2.39	0.88	0.38
Lu	0.59	0.19	0.13	0.34	0.14	0.05
ASI	1.130	0.271	0.256	0.984	1.265	1.227
#mg	0.321	0.678	0.616	0.471	0.666	0.544
Rb/Sr	0.388	0.364	0.377	1.387	0.406	0.188
ΣREE	235.17	75.90	55.96	70.79	275.41	66.80
Eu/Eu*	0.584	0.707	0.891	1.284	0.552	1.010
Ce_N/Yb_N	6.263	7.664	7.239	2.868	37.188	19.836
Th/U	3.516	2.333	4.000	1.962	7.160	6.500
T_{Zr} [°C]	856	N.A.	N.A.	723	N.A.	744

#mg = MgO/(MgO + FeO) in molecular units; Eu/Eu* = Eu/γ(Sm · Gd)

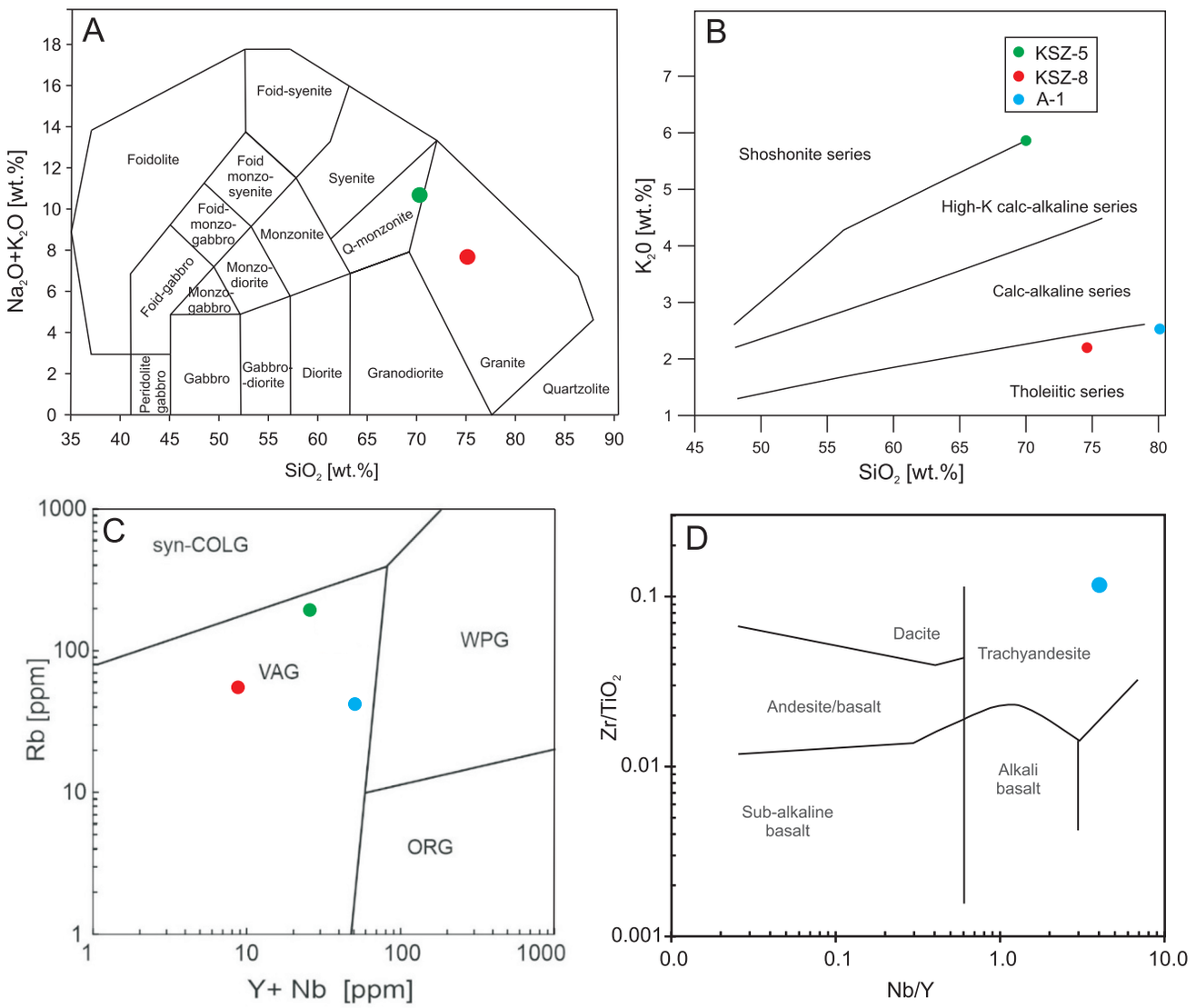

Fig. 4. The igneous exotic blocks from the Janoska Stream plotted on: A – alkali ($Na_2O + K_2O$) *versus* SiO_2 TAS classification diagram after Middlemost (1986); B – K_2O *versus* SiO_2 classification diagram after Peccerillo and Taylor (1976); C – discrimination diagram after Pearce and Harris (1984), VAG – volcanic arc granites, syn-COLG – syn-collision granites, ORG – ocean ridge granites, WPG – within plate granites; D – discrimination diagram after Winchester and Floyd (1977)

tion. Accessory minerals are zircon, rutile, apatite and monazite. Sample is rich in SiO_2 (71 wt.%) and Al_2O_3 (15 wt.%), peraluminous (ASI = 1.27), $Na_2O > K_2O$ with a Rb/Sr ratio = 0.41 (Table 1). Total REE content is high (275 ppm), and shows strong LREE enrichment, with a pronounced negative Eu anomaly (Fig. 5A and Table 1).

Sample KSZ-5 is a dark grey, medium-grained granitoid, composed of K-feldspar, quartz, sericitized plagioclase, sericitized muscovite and biotite (Fig. 3E), with minor secondary carbonate. The accessory minerals are zircon and rutile. The sample has 70% wt. SiO_2, Al_2O_3 (16 wt.%) and K_2O (7 wt.%), is peraluminous (ASI = 0.98), with $K_2O > Na_2O$ and Rb/Sr = 1.39 (Table 1). On the sum of alkalis *versus* SiO_2 plot after Middlemost (1985), it can be classified as quartz-monzonite (Fig. 4A). The sum of REE is 70.79 ppm, while the C1-normalized REE patterns revealed a pronounced positive Eu anomaly of 1.28 and weak REE fractionation (Ce_N/Yb_N = 2.87; Table 1 and Fig. 5A).

ZIRCON AND RUTILE U-Pb GEOCHRONOLOGY

Zircon crystals from two sandstones (KSZ-3, A-2), two granitic exotic clasts (KSZ-5 and KSZ-8), one orthogneiss (A-1) and one paragneiss exotic clast (KSZ-7) from the Istebna Beds (Silesian Nappe) were analyzed. The zircon grains were clear, colourless in sample KSZ-3 and pinkish to yellow in sample A-2, up to 200 μm in length, with aspect ratios of 1:1 to 1:3.

In the two sandstone samples (KSZ-3, A-2) the detrital zircon crystals typically show oscillatory magmatic zoning with variable (strong to weak) cathodoluminescence intensities (Fig. 6A, B), depending on the U content (Appendix 1). Most of the zircon crystals contain partly rounded, inherited cores overgrown by rims showing a variable cathodoluminescence response.

In the sandstone sample A-2, 64 analyses on 49 grains were made. The majority of the zircon population (49 analyses)

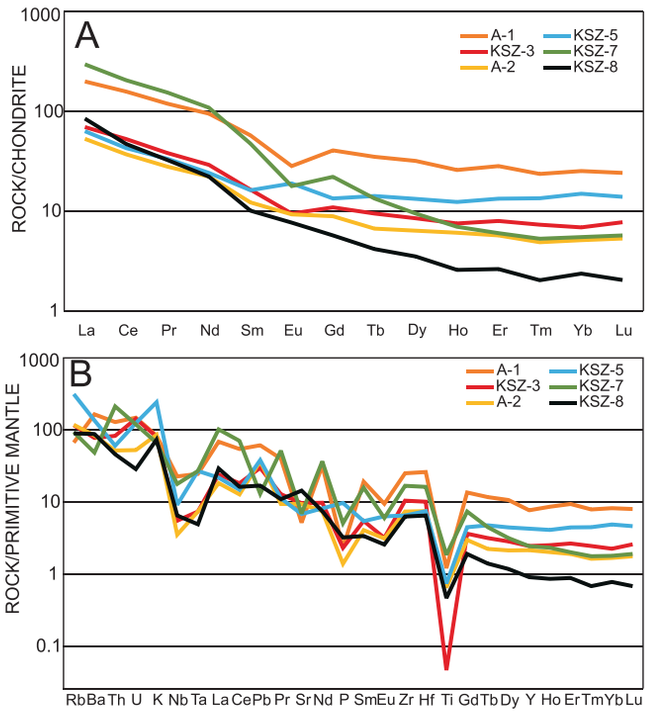

Fig. 5A – chondrite (C1)-normalized REE patterns of the samples; B – primitive mantle normalized multi-element patterns of the analyzed samples from the Janoska Stream

Normalization values after McDonough and Sun (1995)

yielded Variscan ages with a broad spectrum ranging from 311.5 ±3.3 to 391.0 ±9.5 Ma (Fig. 7A). Two concordant cores yielded Neoproterozoic $^{206}Pb/^{238}U$ ages of ~576 and ~596 Ma, three cores yielded Early Paleozoic $^{206}Pb/^{238}U$ ages of ~452, 475 and 508 Ma (Fig. 7A and Appendix 1), while the rest of the analyses (10 points) are discordant (Fig. 7A and Appendix 1).

In the matrix sample KSZ-3, 73 analyses on 50 grains were undertaken. The majority of the zircon population (56 analyses) define a concordia age of 331.7 ±1.1 Ma (Fig. 7C), while the three youngest zircon rims yielded a concordia age of 304.2 ±3 Ma (Fig. 7C). Three inherited cores yielded $^{206}Pb/^{238}U$ ages of ~1754, 2137 Ma and 3050 Ma (Fig. 7C and Appendix 1). Six grains yielded Early Paleozoic (Caledonian?) $^{206}Pb/^{238}U$ ages of between 444 and 500 Ma. Two rims yielded Cadomian $^{206}Pb/^{238}U$ ages of ~615 and 616 Ma (Fig. 7C and Appendix 1) while the rest of the analyses (6 points) are discordant (Fig. 7C and Appendix 1).

In sample A-2, brick-red to dark-brown elongated (1:4), internally homogeneous rutile crystals were found. 27 analyses were undertaken on 27 grains. Four grains were discordant and excluded from calculation, one grain yielded a $^{206}Pb/^{238}U$ age of 414 Ma, while the rest (22) of the analyses yielded a concordia age of 344.7 ±2.5 Ma (Fig. 8 and Appendix 3).

In the granitic samples (KSZ-5 and KSZ-8) oscillatory zoning with variable moderate to weak cathodoluminescence (CL) intensities were typically observed (Fig. 9A, C). Inherited cores, partly rounded, showing both bright and moderate CL responses, corresponding to U enrichment (Appendix 2) and locally with oscillatory zoning, were also found.

In the granite sample KSZ-5, 87 analyses on 42 grains were made. Six rims and cores yielded a concordia age of 325.7 ±2.9 Ma (Fig. 10A; MSWD = 0.7), six zircon grains yielded Eo-Variscan/Caledonian concordant $^{206}Pb/^{238}U$ ages between 365 and 419 Ma (Fig. 10A and Appendix 2), 52 analyses of zircon grains yielded Meso-/Paleoproterozoic $^{206}Pb/^{238}U$ ages between 1166 and 2829 Ma, while the remainder of the analyses (23 points) do not coincide with concordia (Fig. 10A and Appendix 2).

In the granite sample KSZ-8, 55 analyses on 27 grains were made. Six concordant rims yielded a Variscan concordia age of 330.6 ±2.9 Ma (Fig. 10E; MSWD = 0.36). 36 analyses located in grains yielded concordant Neoproterozoic $^{206}Pb/^{238}U$ ages between 546 and 780 Ma, five inherited cores yielded $^{206}Pb/^{238}U$ ages between 1218 and 1671 Ma, while the remainder of the analyses (8 points) are discordant (Fig. 10E and Appendix 2).

Zircon crystals from the paragneiss (KSZ-7) show a great variety of sizes and CL responses (Fig. 9B). While some show the presence of inherited cores rimmed by oscillatory zones, most of the zircons are oscillatory zoned crystals. 41 analyses on 26 grains were made. Most of the grains and rims (37 points) yielded concordant Neoproterozoic $^{206}Pb/^{238}U$ ages between 557 and 686 Ma, one inherited core yielded a $^{206}Pb/^{238}U$ age of 1207 ±33 Ma, with 3 discordant analyses interpreted as Pb loss from the ~1200 Ma age component (Fig. 10C and Appendix 2).

Zircon crystals from the orthogneiss sample (A-1) yielded inherited cores with both dull and bright luminescence, overgrown by oscillatory zoned rims (Fig. 9D). 53 analyses on 42 grains were made. Two concordant rims, with Th/U of 0.79 and 0.05 yielded Variscan $^{206}Pb/^{238}U$ ages of ~337 and ~359 Ma respectively. Two rims with very low Th/U ratios yielded Cadomian $^{206}Pb/^{238}U$ ages of ~527 and 547 Ma (Fig. 10G and Appendix 2), one inherited core yielded a $^{206}Pb/^{238}U$ age of 1896 ±51 Ma, while the remainder of the analyses (48 points) lie on a discordia line with an upper intercept of 1635 ±12 Ma and a poorly constrained lower intercept age of 288 ±100 Ma (MSWD = 4.0; Fig. 10G and Appendix 2).

DISCUSSION

PETROGENETIC INTERPRETATION OF THE CRYSTALLINE ROCK CLASTS

The granitoids from Kamesznica (KSZ-5 and KSZ-8) yield similar concordia ages (325.7 and 330.6 Ma; Fig. 10A, E), with similar slightly positive Eu anomalies (Fig. 5A). However, the granitic rock KSZ-5 lies on the border between high-K calc-alkaline and shoshonite series, while granitoid KSZ-8 belongs to tholeitic

Table 2

Sm-Nd whole-rock isotopic data from the granitoid KSZ-8 from Kamesznica

Isotope data	$^{147}Sm/^{144}Nd$	±2sm	$^{143}Nd/^{144}Nd$	±2sm	Nd_{ini} ^{330}	Nd_{330}	T_{DM}
KSZ-8	0.089171	0.000002	0.511791	0.000002	0.511599	–12.0	1.98

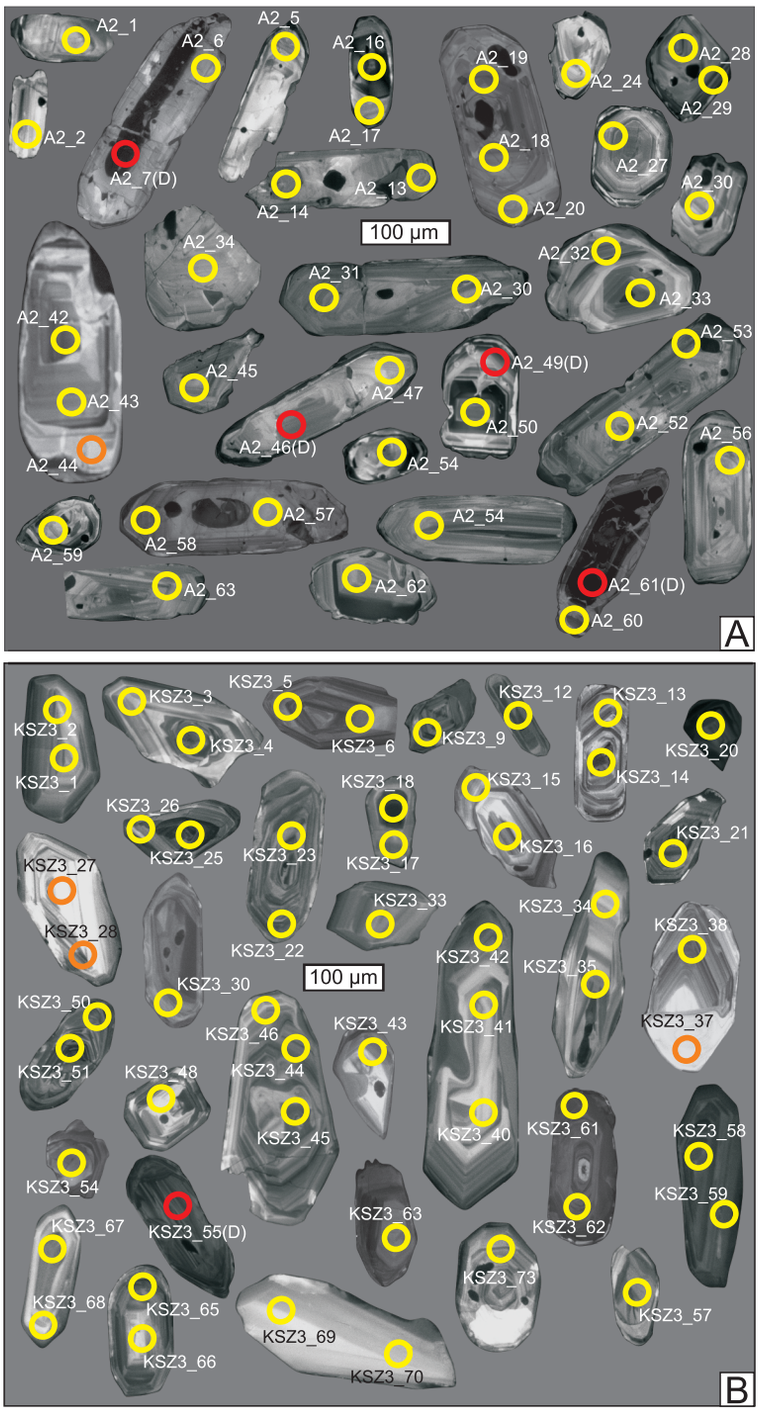

Fig. 6. Cathodoluminescence (CL) images of selected zircon crystals from: A – sandstone (A-2) and B – matrix of conglomerate (KSZ-3) from the Janoska Stream; selected analytical spots and analysis numbers (see Appendix 1) are marked as circles; red circles mean discordant points

series (Fig. 4B). Their peraluminous character and relatively low magmatic crystallization temperatures (Table 1) suggest the partial melting of the sedimentary protolith and is supported by the negative εNd_{330} = –12 (Table 2). In both granitoids the Proterozoic is the dominant age component (Neoproterozoic for KSZ-8 and Meso- and Paleoproterozoic for KSZ-5). Both granitoids can be classified as volcanic arc-related magmas (Fig. 4C). The primitive-mantle-normalized multi-element plots for both samples (Fig. 5B) points also to an arc-setting, with characteristic negative Nb and Ta anomalies and negative P and Ti anomalies which can imply a significant crustal component in the parent melt. However, all these features can be also a result of inheritance from primary metasedimentary source rocks within a volcanic arc regime (see Gawęda et al., 2005 for comparison). The latter suggestion looks probable in the light of the abundance of inherited zircon cores of Neo-, Meso- and Paleoproterozoic age (Fig. 10A and Appendix 2) and a T_{DM} age of and 1.98 Ga for the KSZ-8 granitoid (Table 2). The gneissic clast (KSZ-7) may represent the metamorphic envelope rock to the granites, and was likely metamorphosed in the late Neoproterozoic (550–640 Ma; Fig. 10C).

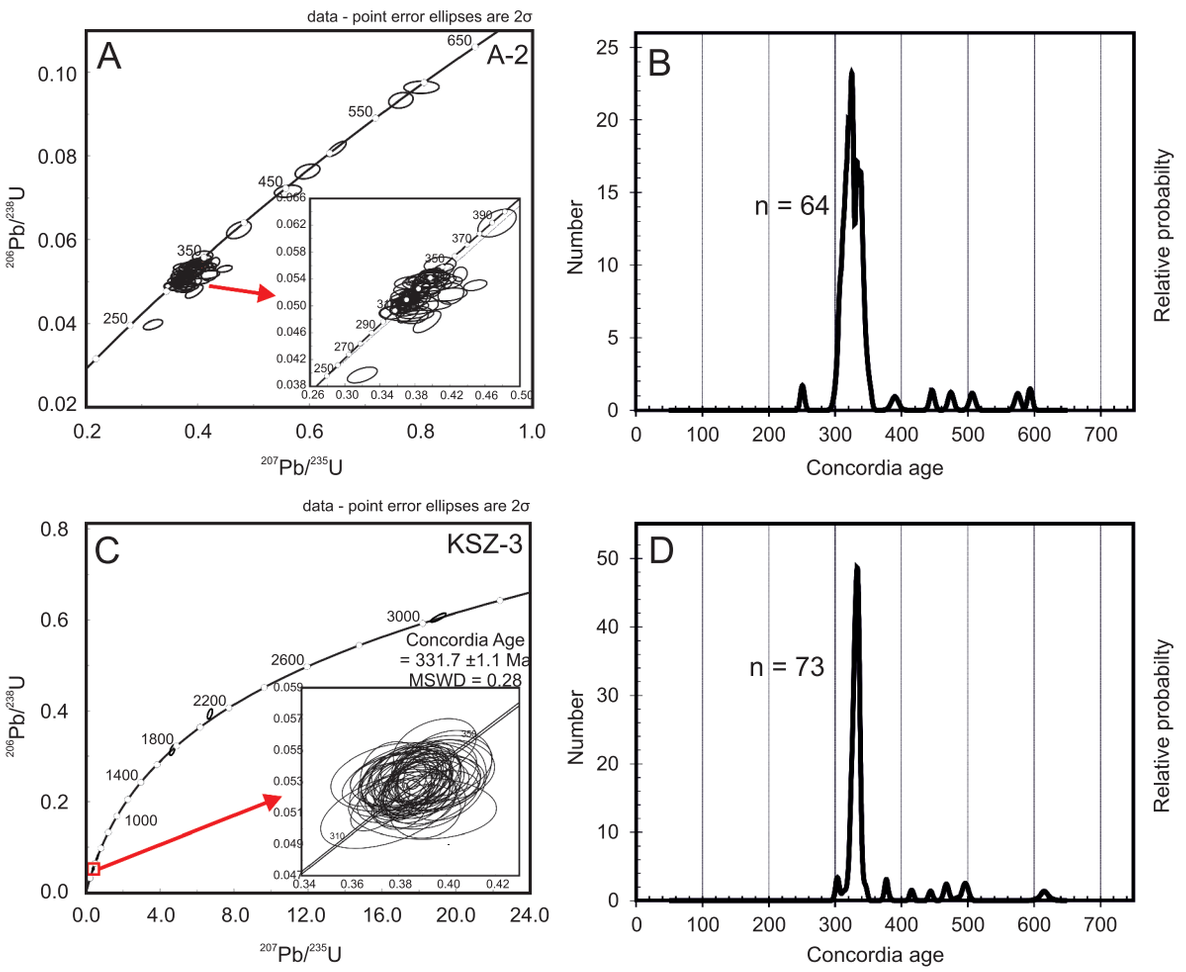

Fig. 7. Concordia plots of LA-ICP-MS U-Pb zircon data: A – sandstone (A-2) with insert of intercept age (order after profile); C – matrix of conglomerate (KSZ-3) with insert of Variscan grains; and density plots of: B – sandstone (A-2) and D – matrix of conglomerate (KSZ-3)

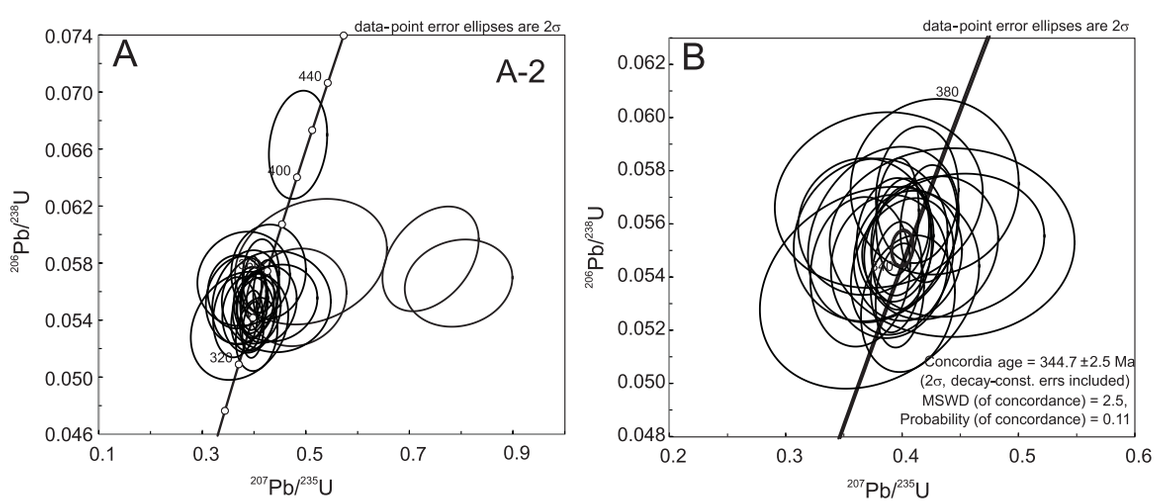

Fig. 8. Concordia plots of LA-ICP-MS rutile analytical results from (A) A-2 sandstone with (B) insert of youngest concordant data

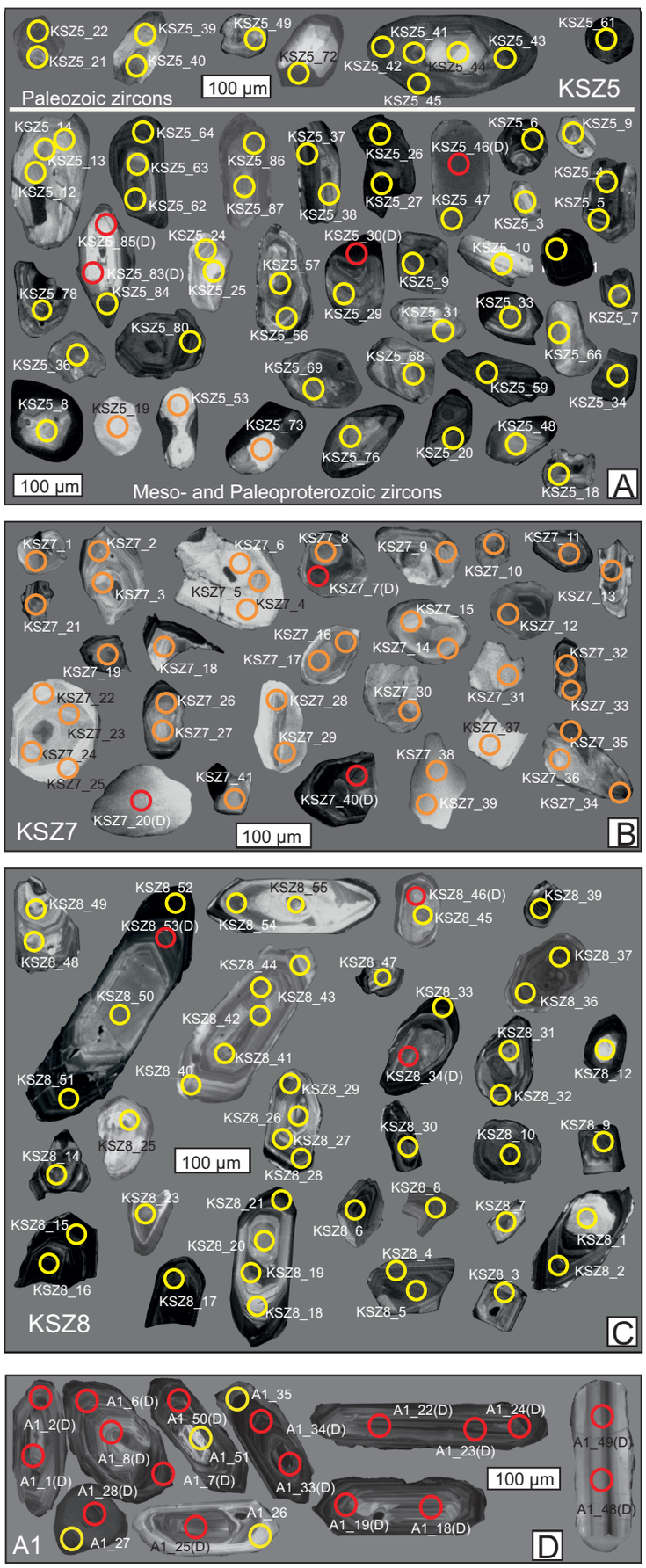

Fig. 9. Cathodoluminescence (CL) images of selected zircon crystals from: A – granitoid clast (KSZ-5); B – paragneiss clast (KSZ-7); C – granitoid clast (KSZ-8) and D – orthogneiss clast (A-1) from the Janoska Stream

Selected analytical spots and analysis numbers (see Appendix 2) are marked as circles; red circles mean discordant points

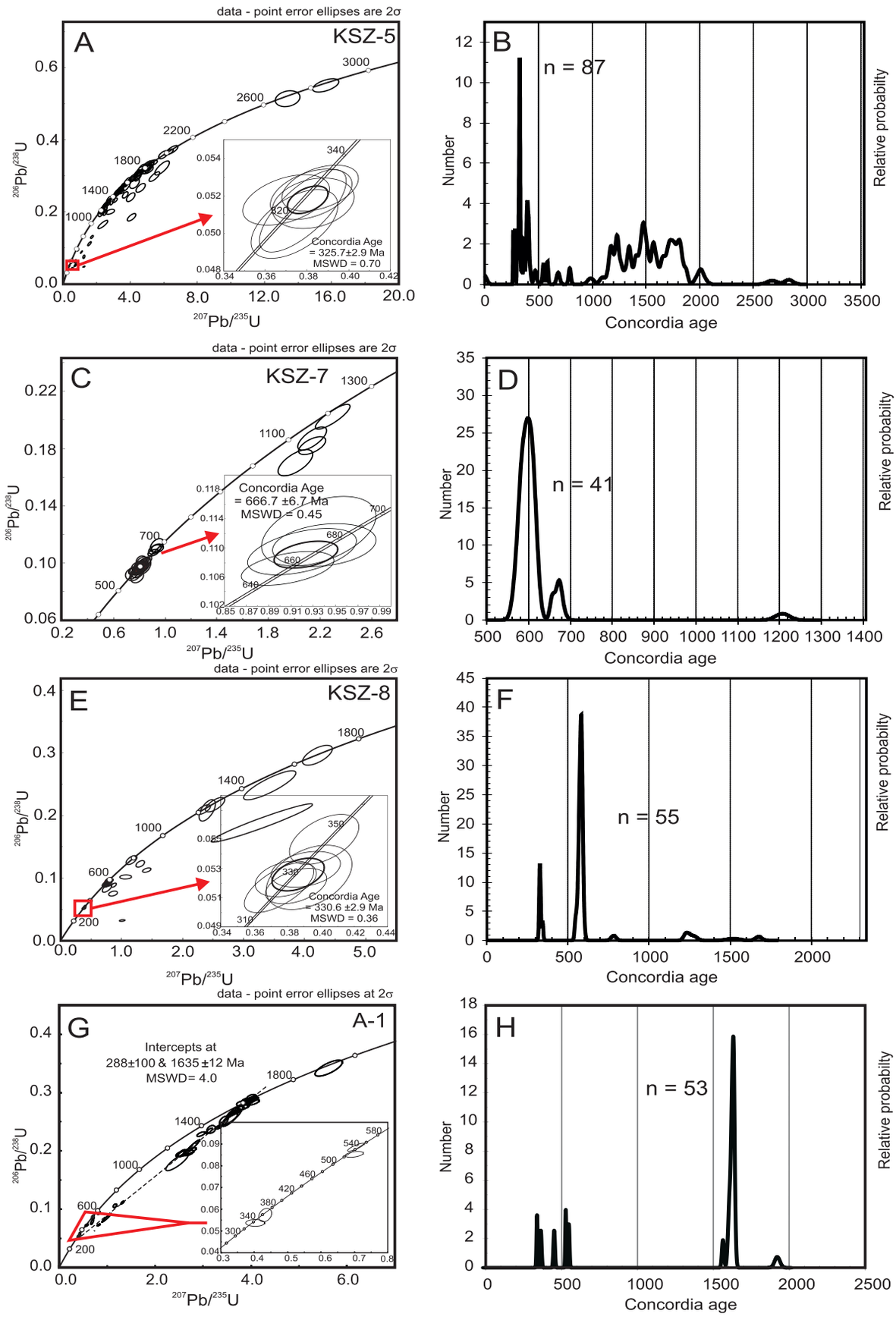

Fig. 10. Concordia plots of LA-ICP-MS zircon analytical results: A – granitoid (KSZ-5) with insert of Variscan grains; C – paragneiss (KSZ-7) with insert of Neoproterozoic grains; E – granitoid (KSZ-8) with insert of Variscan rims; G – orthogneiss (A-1) with insert of Variscan and Cadomian rims and density plots of analysed samples: B – granitoid (KSZ-5); D – paragneiss (KSZ-7); F – granitoid (KSZ-8); H – orthogneiss (A-1)

The major element geochemistry of the A-1 orthogneiss sample is likely modified due to secondary quartz remobilization and crystallization. The trace element characteristics imply a trachyandesite magmatic protolith (Fig. 4D) after Winchester and Floyd (1977). The primitive-mantle normalized multi-element plot (Fig. 5B) shows both negative Ta and Nb anomalies as well as negative P and Ti anomalies, implying a volcanic arc environment, which agrees with its affinity on a geotectonic discrimination diagram (Fig. 4C) after Pearce et al. (1984). The upper intercept U-Pb age of ~1635 Ma (Fig. 10G) is interpreted as the crystallization age of the trachyandesitic magma. Two rims dated at ~527 and 547 Ma (Fig. 10G) are interpreted as reflecting a post-Cadomian episode of recrystallization, with very low Th/U ratios (<0.01; Appendix 2), implying a metamorphic/hydrothermal overprint. Two rims dated at ~337 and 359 Ma (Fig. 10G), with Th/U ratios of 0.79 and 0.05 respectively imply zircon growth under both magmatic and metamorphic/hydrothermal conditions. The poorly constrained lower intercept age of 288 ±100 Ma on grains characterized by Th/U ratios varying from 0.92 to 0.01 (Appendix 2), provides supporting evidence for a Variscan high-temperature overprint associated with late Variscan magmatic activity in Central Europe (cf. Mazur et al., 2020; Golonka et al., 2021b).

INTERPRETATION OF DETRITAL ZIRCON SPECTRA FROM THE SEDIMENTARY ROCKS

The detrital zircon age spectra of the KSZ-3 (conglomerate matrix) and A-2 (sandstone) samples, as well as of rutile from the A-2 sample are similar with Variscan peaks (Fig. 7B, D) and detrital pre-Variscan (406–508 Ma) inherited cores/crystals. The Variscan zircons in sample KSZ-3 (331.7 ±1.1; Fig. 7C and Appendix 1) show a wide range of U and Th concentrations, CL intensities (Fig. 6A) and Archean, Paleo- and Meso-Proterozoic cores are present but rare (similar to the age spectrum in the A-1 orthogneiss sample). There is a lack of zircon cores older then Neoproterozoic in the A-2 sandstone sample, and some of the grains are also non-magmatic, as concluded from low Th/U ratios (<0.01; see Rubatto, 2002). The rutile age spectrum in the A-2 sandstone sample is similar to that of zircon.

PALAEOGEOGRAPHIC INTERPRETATION

The Silesian Ridge was a NW-SE trending basement high, roughly parallel to the margin of the East European Platform, and it separated the Magura and Silesian basins (Fig. 2). It was the locus of turbidity currents and debris flows in the Late Cretaceous-Paleogene time interval (Poprawa et al., 2004; Cieszkowski et al., 2012; Golonka et al., 2019). The larger crystalline clasts were likely derived directly from the eroded Silesian Ridge (from the SW). The material forming the matrix of the sandstones and interleaved conglomerates was derived partly from the same source and partly from recycled material transported by currents lateral to the Silesian Ridge and European Platform (from the NW) (Golonka et al., 2019).

In the sandy-conglomerate cohesive debrite, the matrix (KSZ-3) represents the erosion stage of the metamorphic rocks enveloping the granitoid pluton(s). The overlying sandstone A-2 contains both a zircon fraction from the same source and a Variscan zircon fraction, delivered from the NW, which are undistinguishable from each other. Progressive erosion exposed the granitoid cores, represented by the KSZ-5 and KSZ-8 samples and their metamorphic envelope (KSZ-7).

Notably, this is the first record of exotic clasts of Meso-Variscan age (KSZ-8, ~330 Ma) inside the Silesian Nappe, as up to now the exotic block population in the Silesian and Subsilesian nappes has been dominated by Neoproterozoic magmatic and metamorphic clasts with the exception of one location in Pluskawka (Subsilesian Nappe) where subvolcanic late Variscan (293 to ~310 Ma) exotic blocks have been found (compare Poprawa et al., 2004; Budzyń et al., 2011; Gawęda et al., 2019a; Burda et al., 2019; Golonka et al., 2021b). The samples in this study (Janoska stream) may represent either the western zone of the Silesian Ridge, where tectonic exhumation exposed deeply located granitoid plutons or a Variscan collisional suture, exposed during Alpine tectonic movements.

The geochemical and isotopic characteristics of the two granitoid samples imply melting of a metasedimentary protolith of Paleoproterozoic age (T_{DM} age = 1.98 Ga). T_{DM} ages of Variscan plutons in Europe are usually in the range of 1.1–1.7 Ga (Liew and Hoffman, 1988; Gawęda et al., 2019b) and such model ages are not interpreted to record a geological event as they result from mixing of melted sources (compare Moyen et al. 2017 and references therein). The analysed exotic clasts of Variscan granite are different to the classic European model; they do not represent young magmas but rather recycled Paleoproterozoic crust of ~1.9 Ga. That allows us to suppose that there was no source mixing, but rather direct melting of Paleoproterozoic crust, metamorphosed in the Neoproterozoic, as shown by the spectrum of inherited cores and the presence of metamorphic clasts (Fig. 10C, D).

CONCLUSIONS

1. The source area of eroded material, the western Silesian Ridge, was built of Meso-Variscan granitoid rocks and their metamorphic country rock, as documented both by the exotic clasts and detrital zircon/rutile analyses. That is the first evidence of Meso-Variscan granitoid activity in the crystalline basement of the Silesian Ridge and in the whole Protocarpathians.

2. The granitoids represent the partial melts of a sedimentary protolith and yield concordia ages of 325.7 ±2.9 Ma and 330.6 ±2.9 Ma. Probably there was no source mixing but original Paleoproterozoic crust (T_{DM} = 1.98 Ga) was melted.

3. The metamorphic country rocks (both ortho- and paragneisses) yield Meso-Proterozoic protolith ages, with Neoproterozoic prolonged metamorphism and locally also late Variscan re-heating.

Acknowledgements. This study was supported by National Science Centre (NCN) grant 2016/23/B/ST10/01896 given to J.G., AGH statutory fund no. 16.16.140.315 (M.Sz.) and internal project of INoZ UŚ (A.G., K.Sz.). D.C. acknowledges past and present support from Science Foundation Ireland (SFI) through research grants 12/IP/1663, 13/RC/2092 and 13/RC/2092_P2 (iCRAG Research Centre), and 15/IA/3024. iCRAG is funded under the SFI Research Centres Programme. The authors thank A. Zagórska for her help with heavy minerals separation, while M. Horschinegg is acknowledged for the help in the Nd isotope whole-rock work.

REFERENCES:

Bracciali, L., Parrish, R.R., Horstwood, M.S.A., Condon, D.J., Najman, Y., 2013. U-Pb LA-(MC)-ICP-MS dating rutile: New reference materials and applications to sedimentary provenance. Chemical Geology, **347**: 82–101.

Budzyń, B., Dunkley, D.J., Kusiak, M.A., Poprawa, P., Malata, T., Skiba, M., Paszkowski, M., 2011. SHRIMP U-Pb zircon chronology of the Polish Western Outer Carpathians source areas. Annales Societatis Geologorum Poloniae, **81**: 161–171.

Burda, J., Woskowicz-Ślęzak, B., Klötzli, U., Gawęda, A., 2019. Cadomian protolith ages of exotic mega blocks from Bugaj and Andrychów (Western Outer Carpathians, Poland) and their paleogeographic significance. Geochronometria, **46**: 25–36.

Burtan, J., Nescieruk, P., Wójcik, A., 2016. Objaśnienia do Szczegółowej Mapy Geologicznej Polski w skali 1:50 000, arkusz Wisła (in Polish). Państwowy Instytut Geologiczny, Warszawa.

Chew, D.M., Petrus, J.A., Kamber, S., 2014. U-Pb LA-ICPMS dating using accessory mineral standards with variable common Pb. Chemical Geology, **363**: 185–199.

Chew, D., O'Sullivan, G., Caracciolo, L., Mark, C., Tyrrell, S., 2020. Sourcing the sand: accessory mineral fertility, analytical and other biases in detrital U-Pb provenance analysis**.** Earth-Science Reviews, **202:** 103093.

Cieszkowski, M., Golonka, J., Ślączka, A., Waśkowska, A., 2012. Role of the olistostromes and olistoliths in tectonostratigraphic evolution of the Silesian Basin in the Outer Carpathians. Tectonophysics, **568–569**: 248-265.

Eliáš, M., Vašíček, Z., Skupien, P., 2003. Základní rysy pozdněj-urske a spodnokřidove sedimentace ve slezské jednotce na české, územi (vnější Západní Karpaty) (in Czech). Sbornik vědeckých. Prací Vysoké Školy báňské –TU, Řada horonicko-geologická, Monografie, **8**: 117–126.

Gawęda, A., Doniecki, T., Burda, J., Kohut, M., 2005. The petrogenesis of quartz-diorites from the Tatra Mountains (Central Western Carpathians): an example of magma hybridisation. Neues Jahrbuch für Mineralogie Abhandlungen, **181**: 95–109.

Gawęda, A., **Golonka, J., 2011**. Variscan plate dynamics in the circum-Carpathian area. Geodinamica Acta, **24**: 141–155.

Gawęda, A., Golonka, J., Waśkowska, A., Szopa, K., Chew, D., Starzec, K., Wieczorek, A., 2019a. Neoproterozoic crystalline exotic clasts in the Polish Outer Carpathian flysch: remnants of the Proto-Carpathian continent? International Journal of Earth Sciences, **108**: 1409-1427.

Gawęda, A., Szopa, K., Włodyka, R., Burda, J., Crowley, Q., Sikorska, M., 2019b. Continuous magma mixing and cumulate separation in the High Tatra Mountains open system granitoid intrusion, Western Carpathians (Poland/Slovakia): a textural and geochemical study. Acta Geologica Polonica, **69**: 549-570.

Geroch, S. 1960. Microfaunal assemblages from the Cretaceous and Paleogene Silesian Unit in the Beskid Śląski Mts. (Western Carpathians) (in Polish with English summary). Biuletyn Instytutu Geologicznego, **153**: 7-138.

Golonka, J., Picha, F.J., 2006. Introduction. AAPG Memoir, **84**: 1–9.

Golonka, J., Krobicki, M., Oszczypko, N., Ślączka, A., Słomka, T., 2003. Geodynamic evolution and paleogeography of the Polish Carpathians and adjacent areas during Neo-Cimmerian and preceding events (latest Triassic-earliest Cretaceous). Geological Society Special Publications, **208**: 137–158.

Golonka, J., Krobicki, M., Matyszkiewicz, J., Olszewska, B., Ślączka, A., Słomka, T., 2005. Geodynamics of ridges and development of carbonate platform within the Carpathian realm in Poland. Slovak Geological Magazine, **11**: 5–16.

Golonka, J., Krobicki, M., Słomka, T., Oszczypko, N., Ślączka, A., 2006. Jurassic geodynamics of ridges within the Outer Carpathian realm in Poland. Volumina Jurassica, **4**: 42–43.

Golonka, J., Ślączka, A., Waśkowska, A., Krobicki, M., Cieszkowski, M., 2013. Budowa geologiczna zachodniej części polskich Karpat zewnętrznych (in Polish). In: V Polish Sedimentology Conference POKOS 5'2013, Głębokomorska sedymentacja fliszowa – sedymentologiczne aspekty historii basenów karpackich (eds. M. Krobicki and A. Feldman-Olszewska), 16–19.05.2013, Żywiec, 11–62.

Golonka, J., Waśkowska, A., Ślączka, A., 2019. The Western Outer Carpathians: origin and evolution. Zeitschrift der Deutschen Gesellschaft für Geowissenschaften, **170**: 229–254.

Golonka, J., Gawęda, A., Waśkowska, A., 2021a. Carpathians. In: Encyclopedia of Geology, 2nd Ed. (eds. D. Alderon and S.A. Elias): 372–381. Elsevier, Amsterdam.

Golonka, J., Gawęda, A., Waśkowska, A., Chew, D., Szopa, K., Foteini, D., 2021b. Tracing pre-Mesozoic tectonic sutures in the crystalline basement of the Protocarpathians: evidence from the exotic blocks from Subsilesian Nappe, Outer Western Carpathians, Poland. Minerals, **11**: 571.

Kennedy, A.K., Wotzlaw, J-F., Schaltegger, U., Crowley, J.L., Schmitz, M., 2014. Eocene zircon reference material for microanalysis of U-Th-Pb isotopes and trace elements. Canadian Mineralogist, **52**: 409–421.

Książkiewicz M. (ed), 1962. Geological Atlas of Poland, Stratigraphic and Facial Problems. Wyd. Geol., Warsaw.

Książkiewicz, M., 1975. Bathymetry of the Carpathian flysch basin. Acta Geologica Polonica, **25**: 309–368.

Książkiewicz, M., 1977. Hypothesis of plate tectonics and the origin of the Carpathians. Annales Societatis Geologorum Poloniae, **47**: 329–353.

Liew, T.C., Hofmann, A.W., 1988. Precambrian crustal components, plutonic associations, plate environment of the Hercynian Fold Belt of Central Europe: Indications from a Nd and Sr isotopic study. Contributions to Mineralogy and Petrology, **98**: 129–138.

Ludwig, K.R., 2012. Isoplot/Ex, v. 3.75. Berkeley Geochronology Center Special Publication, **5**.

Mark, C., Cogné, N., Chew, D., 2016. Tracking exhumation and drainage divide migration of the Western Alps: a test of the apatite U-Pb thermochronometer as a detrital provenance tool. GSA Bulletin, **128**: 1439–1460.

Mazur, S., Aleksandrowski, P., Gągała, Ł., Krzywiec, P., Żaba, J., Gaidzik, K., Sikora, R., 2020. Late Paleozoic strike-slip tectonics versus oroclinal bending at the SW outskirts of Baltica: case of the Variscan belt's eastern end in Poland. International Journal of Earth Sciences, **109**: 1133–1160.

McDonough, W.F., Sun, S.S., 1995. The composition of the Earth. Chemical Geology, **120**: 223–253.

Middlemost, E.A.K., 1985. Magmas and Magmatic Rocks: an Introduction to Igneous Petrology. Longman Group Ltd., London, UK.

Moyen, J.F., Laurent, O., Chelle-Michou, C., Couzinié, S., Vanderhaege, O., Zeh, A., Villaros, A., Gardien, V., 2017. Collision vs. subduction-related magmatism: two contrasting ways of granite formation and implications for crustal growth. Lithos, **277**: 154–177.

O'Sullivan, G.J., Chew, D.M., Samson, S.D., 2016. Detecting magma-poor orogens in the detrital record. Geology, **44**: 871–874.

Oszczypko, N., 2004. The structural position and tectonosedimentary evolution of the Polish Outer Carpathians. Przegląd Geologiczny, **52**: 780–791.

Oszczypko, N., 2006. Late Jurassic-Miocene evolution of the Outer Carpathian fold-and-thrust belt and its foredeep basin (Western Carpathians, Poland). Geological Quarterly, **50** (1): 169–194.

Paton, C., Hellstrom, J., Paul, B., Woodhead, J., Hergt, J., 2011. Iolite: Freeware for the visualisation and processing of mass spectrometric data. Journal of Analytical Atomic Spectrometry, **26**: 2508–2518.

Pearce, J.A., Harris, N.B.W., Tindle, A.G., 1984. Trace elements discrimination diagram for the tectonic interpretation of granitic rocks. Journal of Petrology, **25**: 956–983.

Peccerillo, A., Taylor, S.R., 1976. Geochemistry of Eocene calc-alkaline volcanic rocks from the Kastamonu area, Northern Turkey. Contributions to Mineralogy and Petrology, **58**: 63–81.

Petrus, J.A., Kamber, B.S., 2012. VizualAge: a novel approach to laser ablation ICP-MS U-Pb geochronology data reduction. Geostandards and Geoanalytical Research, **36**: 247–270.

Pointon, M.A., Cliff, R.A., Chew, D.M., 2012. The provenance of Western Irish Namurian Basin sedimentary strata inferred using detrital zircon U–Pb LA-ICP-MS geochronology. Geological Journal, **47**: 77–98.

Poprawa, P., Malata, T., Pécskay, Z., Banaś, M., Skulich, J., Paszkowski, M., Kusiak, M., 2004. Geochronology of the crystalline basement of the Western Outer Carpathians` sediment source area – preliminary data. Mineralogical Society of Poland – Special Papers, **24**: 329–332.

Rubatto, D., 2002. Zircon trace element geochemistry: partitioning with garnet and the link between U-Pb ages and metamorphism. Chemical Geology, **184**: 123–138.

Ryłko, W., 2019. Objaśnienia do Szczegółowej Mapy Geologicznej Polski w skali 1:50 000, arkusz Milówka (in Polish). Państwowy Instytut Geologiczny, Warszawa.

Schmitt, A.K., Zack, T., 2012. High-sensitivity U–Pb rutile dating by secondary ion mass spectrometry (SIMS) with an O_2^+ primary beam. Chemical Geology, **332-333**: 65–73.

Sláma, J., Košler, J., Condon, D.J., Crowley, J.L., Gerdes, A., Hanchar, J.M., Schaltegger, U., 2008. Plešovice zircon – a new natural reference material for U-Pb and Hf isotopic microanalysis. Chemical Geology, **249**: 1–35.

Stacey, J.S., Kramers, J.D., 1975. Approximation of terrestrial lead isotope evolution by a two-stage model. Earth and Planetary Science Letters, **26**: 207–221.

Starzec, K., Golonka, J., Waśkowska, A., 2017. Zespół form skałkowych na Karolówce w Istebnej (Beskid Śląski, Zachodnie Karpaty Zewnętrzne) – godne ochrony stanowisko z unikatowym materiałem egzotycznym. (in Polish). Chrońmy Przyrodę Ojczystą, **73**: 271–283.

Strzeboński, P., 2005. Cohesive debrites of the Istebna Beds (Upper Senonian – Paleocene) West of the Skawa River (in Polish with English summary). Geologia: Kwartalnik Akademii Górniczo-Hutniczej im. Stanisława Staszica w Krakowie, **31**: 201–224.

Strzeboński, P., 2015. Late Cretaceous-Early Paleogene sandy-to-gravelly debris flows and their sediments in the Silesian Basin of the Alpine Tethys (Western Outer Carpathians, Istebna Formation). Geological Quarterly, **59** (1): 195–214.

Sun, W., McDonough, W.F., 1989. Chemical and isotopic systematics of oceanic basalts: implications for mantle composition and processes. Geological Society Special Publications, **42**: 313–345.

Ślączka, A., Kruglow, S., Golonka, J., Oszczypko, N., Popadyuk, I., 2006. The general geology of the Outer Carpathians, Poland, Slovakia, and Ukraine. AAPG Memoir, **84**: 221–258.

Unrug, R., 1963. Istebna Beds – a fluxoturbidity formation in the Carpathian Flysch. Annales Societatis Geologorum Poloniae, **33**: 49–92.

Unrug, R., 1968. The Silesian cordillera as the source of clastic material of the flysch sandstone of the Beskid Śląski and Beskid Wyspowy ranges (Polish Western Carpathians) (in Polish with English summary). Annales Societatis Geologorum Poloniae, **38**: 155–164.

Wiedenbeck, M., Alle, P., Corfu, F., Griffin, W.L., Meier, M., Oberli, F.V., Spiegel, W., 1995. Three natural zircon standards for U-Th-Pb, Lu-Hf, trace element and REE analyses. Geostandards and Geoanalytical Research, **19**: 1–23.

Wiedenbeck, M., Hanchar, J.M., Peck, W.H., Sylvester, P., Valley, J., Whitehouse, M., Kronz, A., Morishita, Y., Nasdala, L., Fiebig, J., Franchi, I., Girard, J.-P., Greenwood, R.C., Hinton, R., Kita, N., Mason, P.R.D., Norman, M., Ogasawara, M., Piccoli, P.M., Rhede, D., Satoh, H., Schulz-Dobrick, B., Skår, O., Spicuzza, M.J., Terada, K., Tindle, A., Togashi, S., Vennemann, T., Xie, Q., Zheng, Y.-F., 2004. Further characterization of the 91500 zircon crystal. Geostandards and Geoanalytical Research, **28**: 9–39.

Winchester, J.A., Floyd, P.A., 1977. Geochemical discrimination of different magma series and their differentiation products using immobile elements. Chemical Geology, **20**: 325–343.

Zack, T., Stockli, D.F., Luvizotto, G.L., Barth, M.G., Belousova, E., Wolfe, M.R., Hinton, R.W., 2011. In situ U-Pb rutile dating by LA-ICP-MS: ^{208}Pb correction and prospects for geological applications. Contributions to Mineralogy and Petrology, **162**: 515–530.

APPENDIX 1 LA-ICP-MS U-Pb detrital zircon data from the Janoska stream, Outer Western Carpathians, SW-Poland

Sample ID	Final207_235	2 s	Final206_238	2 s	ErrorCorrelation_6_38	FinalAge206_238	2 s	FinalAge207_235	2s	FinalAge207_206	2s	U [ppm]	Th [ppm]	Th/U
Sandstone														
Neoproterozoic detrital cores														
A2_42	0.801	0.026	0.096	0.001	0.047	593	7.4	597	19.4	622	22	134	139	1.031
A2_59	0.764	0.018	0.093	0.002	0.201	575	9.2	576	13.6	585	15	1105	4700	4.253
Lower Paleozoic detrital cores														
A2_16	0.649	0.014	0.082	0.002	0.753	506	9.3	508	11.0	522	14	909	359	0.395
A2_33	0.597	0.018	0.076	0.001	0.343	474	8.7	475	14.3	503	16	1016	86	0.084
A2_50	0.562	0.020	0.072	0.001	0.268	446	7.5	453	16.1	464	16	544	3210	5.901
Variscan crystal and rims (concordant)														
A2_54	0.474	0.018	0.062	0.002	0.456	390	10.6	394	15.0	392	18	208	378	1.816
A2_10	0.413	0.010	0.055	0.001	0.354	347	4.5	351	8.3	379	9.1	699	68	0.098
A2_2	0.409	0.015	0.056	0.001	0.173	352	6.0	348	12.8	316	12	566	219	0.387
A2_28	0.402	0.009	0.055	0.001	0.337	344	4.5	343	7.9	346	7.8	340	231	0.679
A2_1	0.402	0.015	0.054	0.001	0.034	341	4.6	343	12.8	392	16	158	37	0.236
A2_4	0.401	0.013	0.055	0.001	0.001	343	4.4	342	11.1	371	14	263	24	0.091
A2_40	0.400	0.016	0.054	0.001	0.226	338	6.3	342	13.7	346	13	253	553	2.186
A2_12	0.399	0.007	0.054	0.001	0.412	339	3.2	341	5.9	358	6.1	595	15	0.026
A2_18	0.398	0.024	0.054	0.001	0.204	338	5.5	340	20.5	371	22	143	84	0.590
A2_14	0.397	0.016	0.053	0.001	0.155	336	4.2	339	13.7	371	14	212	229	1.080
A2_45	0.396	0.009	0.054	0.001	0.001	339	3.6	339	7.6	346	9.1	597	406	0.680
A2_8	0.396	0.014	0.054	0.001	0.282	338	5.8	339	12.0	371	13	160	24	0.148
A2_56	0.395	0.015	0.054	0.001	0.533	338	7.5	338	12.8	367	12	459	1.0	0.002
A2_38	0.394	0.023	0.053	0.001	0.001	335	5.7	337	19.7	392	24	220	443	2.014
A2_19	0.392	0.014	0.052	0.001	0.352	326	4.6	336	12.0	371	13	463	641	1.384
A2_34	0.390	0.011	0.053	0.001	0.563	332	5.6	334	9.4	358	8.7	567	150	0.265
A2_57	0.390	0.014	0.054	0.001	0.540	340	4.6	334	12.0	333	11	371	2000	5.391
A2_6	0.389	0.007	0.053	0.001	0.276	331	3.6	334	6.3	367	7.5	1976	67	0.034
A2_52	0.388	0.009	0.053	0.000	0.250	332	3.0	333	7.4	337	7.6	842	0.0	0.000
A2_31	0.386	0.009	0.053	0.001	0.076	332	4.1	332	7.5	346	8.4	405	294	0.726
A2_5	0.385	0.024	0.053	0.001	0.281	331	6.1	331	20.6	294	19	78	0.7	0.009
A2_11	0.385	0.009	0.052	0.001	0.145	327	4.4	331	8.1	350	8.5	802	36	0.045
A2_58	0.385	0.019	0.052	0.001	0.438	327	4.3	331	16.3	371	18	246	4900	19.919
A2_21	0.385	0.009	0.052	0.001	0.216	327	3.3	331	7.6	354	7.3	760	1270	1.671
A2_24	0.380	0.015	0.051	0.001	0.459	319	6.9	327	12.9	384	13	539	502	0.931
A2_13	0.379	0.010	0.052	0.000	0.272	324	3.1	326	8.6	367	8.8	1136	87	0.076
A2_22	0.379	0.011	0.052	0.001	0.076	324	4.1	326	9.5	354	9.3	797	274	0.344
A2_15	0.377	0.014	0.049	0.001	0.153	307	4.0	325	12.1	424	15	535	90	0.169
A2_51	0.377	0.014	0.051	0.001	0.333	320	7.5	325	12.1	358	14	635	0.0	0.000
A2_60	0.377	0.015	0.049	0.001	0.042	306	6.3	325	12.9	484	17	296	832	2.811
A2_3	0.376	0.012	0.051	0.001	0.566	321	5.2	324	10.3	346	9.7	445	72	0.161
A2_64	0.375	0.017	0.050	0.001	0.001	315	4.5	323	14.7	404	21	184	430	2.342
A2_27	0.375	0.015	0.053	0.001	0.222	336	4.7	323	12.9	232	9.1	130	174	1.338
A2_41	0.375	0.009	0.051	0.001	0.022	323	4.1	323	7.8	325	8.0	528	306	0.580
A2_17	0.375	0.010	0.051	0.000	0.317	320	3.0	323	8.5	342	7.7	1100	2470	2.245
A2_30	0.375	0.008	0.052	0.001	0.130	326	3.4	323	6.5	333	7.5	609	375	0.616
A2_39	0.373	0.011	0.051	0.001	0.298	319	4.0	322	9.5	358	11	911	486	0.533
A2_55	0.372	0.010	0.050	0.001	0.247	315	5.3	321	8.6	384	8.5	788	0.0	0.000
A2_37	0.372	0.010	0.049	0.001	0.651	306	5.4	321	8.2	432	9.3	1212	187.5	0.155
A2_32	0.370	0.010	0.051	0.001	0.266	319	4.2	320	8.6	346	9.1	498	442	0.888
A2_20	0.368	0.014	0.049	0.001	0.087	311	4.7	318	12.1	337	13	237	450	1.899
A2_53	0.368	0.011	0.050	0.001	0.288	312	3.6	318	9.5	363	10	1852	0.0	0.000
A2_43	0.367	0.012	0.052	0.001	0.182	324	4.9	317	10.4	281	8.7	205	278	1.356
A2_47	0.366	0.012	0.051	0.001	0.287	321	3.8	317	10.4	285	9.3	293	1457	4.979
A2_48	0.366	0.010	0.050	0.001	0.066	317	4.1	317	8.7	320	10	729	2277	3.123
A2_44	0.364	0.010	0.049	0.001	0.259	311	3.4	315	8.7	350	9.8	378	668	1.766
A2_63	0.364	0.008	0.050	0.001	0.304	316	3.7	315	7.0	320	7.3	508	703	1.384
A2_62	0.358	0.010	0.050	0.001	0.194	315	4.5	311	8.5	268	6.7	360	246	0.684
A2_29	0.354	0.012	0.049	0.001	0.132	308	5.1	308	10.4	325	13	648	341	0.526
Discordant cores and rims														
A2_7	0.432	0.006	0.055	0.001	0.153	343	5.5	364	5.4	495	9	1127	243	0.216
A2_9	0.449	0.011	0.053	0.001	0.396	333	4.1	377	9.2	632	12	601	156	0.260
A2_23	0.421	0.012	0.052	0.001	0.156	326	8.2	357	10.2	537	13	319	216	0.678
A2_25	0.422	0.010	0.053	0.001	0.283	336	4.4	358	8.3	515	12	798	172	0.216
A2_26	0.320	0.014	0.040	0.001	0.519	251	6.1	282	12.3	503	18	323	291	0.901
A2_35	0.380	0.022	0.050	0.001	0.032	316	7.5	327	18.9	436	24	126	71	0.562
A2_36	0.398	0.019	0.050	0.001	0.281	314	3.6	340	16.2	578	25	273	156	0.572
A2_49	0.371	0.025	0.049	0.001	0.001	308	6.3	320	21.6	408	29	110	2462	22.301
A2_46	0.420	0.016	0.052	0.001	0.302	325	5.0	356	13.6	571	20	1699	678	0.399
A2_61	0.394	0.013	0.048	0.001	0.683	300	8.2	337	11.1	636	18	2001	1427	0.713
Matrix of conglomerate														
Cadomian rims														
KSZ_03_20	0.852	0.042	0.100	0.004	0.411	616	20	624	22	690	95	1529	183	0.120
KSZ_03_62	0.856	0.035	0.100	0.003	0.038	615	9.7	628	17	687	88	243	172	0.708
Paleozoic rims/grains														
KSZ_03_39	0.549	0.013	0.071	0.002	0.408	444	6.4	445	6.7	440	41	414	195	0.472
KSZ_03_16	0.586	0.023	0.075	0.002	0.395	467	7.6	470	13	468	74	146	112	0.767

KSZ_03_45	0.597	0.018	0.075	0.002	0.254	468	6.8	474	10	457	60	241	121	0.500
KSZ_03_63	0.621	0.020	0.079	0.003	0.810	490	17	490	12	493	65	246	260	1.057
KSZ_03_40	0.630	0.019	0.081	0.002	0.503	500	7.0	495	11	497	54	1041	158	0.151
KSZ_03_41	0.630	0.014	0.080	0.002	0.109	495	6.2	497	7.2	501	51	373	186	0.499
Inherited cores														
KSZ_03_18	4.660	0.140	0.313	0.012	0.611	1754	46	1759	22	1783	45	666	40	0.060
KSZ_03_4	6.700	0.150	0.393	0.013	0.571	2137	42	2072	15	2007	35	543	1000	1.842
KSZ_03_38	19.040	0.420	0.605	0.016	0.836	3050	32	3042	17	3042	21	822	376	0.457
Variscan grains														
KSZ_03_50	0.342	0.009	0.048	0.001	0.431	302	5.7	298	6.0	267	56	487	192	0.394
KSZ_03_26	0.349	0.009	0.048	0.001	0.498	304	4.6	305	5.6	303	45	516	201	0.390
KSZ_03_72	0.364	0.017	0.050	0.002	0.728	313	7.2	314	12	337	84	336	174	0.518
KSZ_03_35	0.373	0.010	0.051	0.001	0.561	323	3.7	321	6.7	341	45	207	137	0.661
KSZ_03_68	0.376	0.023	0.051	0.002	0.491	322	9.7	327	15	380	110	836	100	0.120
KSZ_03_34	0.377	0.014	0.053	0.002	0.453	331	5.5	324	10	282	74	750	435	0.580
KSZ_03_21	0.378	0.012	0.052	0.002	0.010	329	5.3	325	7.7	292	71	113	173	1.525
KSZ_03_11	0.378	0.011	0.053	0.002	0.234	333	5.6	325	7.2	253	58	498	161	0.323
KSZ_03_2	0.379	0.013	0.052	0.001	0.466	327	4.4	326	9.1	326	63	355	198	0.558
KSZ_03_6	0.379	0.012	0.053	0.002	0.022	334	9.7	326	7.8	263	87	348	245	0.704
KSZ_03_9	0.379	0.022	0.053	0.002	0.279	335	8.1	326	16	270	130	114	124	1.086
KSZ_03_5	0.380	0.019	0.054	0.002	0.598	336	7.0	327	13	274	91	308	154	0.499
KSZ_03_7	0.381	0.014	0.053	0.002	0.267	333	5.3	328	9.2	311	73	575	386	0.671
KSZ_03_56	0.381	0.009	0.052	0.001	0.186	324	3.3	328	5.7	357	45	657	253	0.384
KSZ_03_61	0.381	0.017	0.053	0.001	0.242	334	4.8	329	12	292	88	1122	162	0.144
KSZ_03_51	0.382	0.010	0.053	0.001	0.190	331	4.2	329	6.3	306	56	944	1520	1.610
KSZ_03_19	0.382	0.012	0.053	0.001	0.429	336	4.8	330	8.5	261	64	373	316	0.847
KSZ_03_32	0.383	0.015	0.053	0.001	0.063	330	4.8	330	11	335	89	542	419	0.773
KSZ_03_53	0.383	0.015	0.053	0.002	0.341	334	5.1	330	9.9	272	71	695	427	0.614
KSZ_03_15	0.384	0.013	0.053	0.002	0.197	335	6.1	330	9.0	329	75	64	84	1.306
KSZ_03_33	0.384	0.010	0.053	0.001	0.210	336	4.2	331	6.3	318	47	78	195	2.510
KSZ_03_43	0.384	0.009	0.053	0.002	0.554	330	5.6	330	5.7	335	43	71	167	2.338
KSZ_03_25	0.385	0.011	0.053	0.002	0.642	331	5.4	331	7.2	351	42	228	268	1.175
KSZ_03_66	0.385	0.009	0.053	0.001	0.413	331	4.6	331	5.7	321	48	309	84	0.270
KSZ_03_8	0.386	0.016	0.053	0.002	0.145	331	6.2	332	11	323	83	809	900	1.112
KSZ_03_65	0.386	0.013	0.053	0.002	0.620	335	6.1	331	9.0	371	59	563	606	1.076
KSZ_03_28	0.386	0.010	0.052	0.001	0.410	329	5.0	331	6.3	347	48	254	102	0.401
KSZ_03_22	0.387	0.022	0.053	0.002	0.094	333	5.9	335	17	340	130	532	56	0.105
KSZ_03_70	0.387	0.017	0.052	0.002	0.029	326	5.9	331	12	350	110	487	69	0.142
KSZ_03_13	0.387	0.009	0.054	0.002	0.544	336	5.3	332	5.6	315	37	1084	75	0.070
KSZ_03_17	0.388	0.012	0.052	0.002	0.217	330	5.8	332	8.0	333	74	766	254	0.332
KSZ_03_31	0.388	0.013	0.052	0.002	0.064	327	5.7	333	9.0	365	73	163	186	1.139
KSZ_03_60	0.388	0.012	0.053	0.002	0.432	332	6.9	333	8.2	359	61	457	266	0.582
KSZ_03_69	0.388	0.011	0.052	0.001	0.359	327	4.7	333	7.3	404	61	66	43	0.658
KSZ_03_30	0.389	0.010	0.053	0.001	0.315	335	4.0	334	6.6	332	54	296	179	0.605
KSZ_03_57	0.390	0.010	0.053	0.001	0.083	335	4.6	334	6.2	320	58	492	120	0.244
KSZ_03_1	0.390	0.014	0.053	0.002	0.027	336	5.7	334	9.3	325	82	415	89	0.215
KSZ_03_48	0.390	0.025	0.051	0.002	0.002	323	7.1	334	17	390	140	194	121	0.624
KSZ_03_36	0.391	0.018	0.054	0.002	0.121	336	6.3	337	12	311	95	316	454	1.437
KSZ_03_42	0.391	0.018	0.052	0.002	0.456	326	6.1	334	12	421	84	767	101	0.131
KSZ_03_71	0.391	0.012	0.051	0.001	0.104	321	4.8	335	8.0	448	74	423	204	0.482
KSZ_03_27	0.392	0.018	0.053	0.002	0.208	333	5.9	337	12	348	93	37	38	1.030
KSZ_03_54	0.392	0.011	0.053	0.002	0.435	335	5.5	336	7.6	375	42	1180	582	0.493
KSZ_03_59	0.392	0.014	0.053	0.001	0.327	331	4.5	335	9.7	365	69	1587	503	0.317
KSZ_03_58	0.392	0.008	0.053	0.001	0.221	334	4.5	336	4.8	348	36	215	184	0.856
KSZ_03_29	0.393	0.011	0.053	0.002	0.275	334	5.1	336	6.9	363	52	247	169	0.686
KSZ_03_52	0.394	0.015	0.054	0.002	0.385	336	6.2	338	9.8	328	77	625	270	0.432
KSZ_03_14	0.395	0.014	0.055	0.002	0.339	346	5.0	339	8.6	251	71	158	109	0.690
KSZ_03_37	0.396	0.016	0.053	0.001	0.230	332	4.9	338	11	396	85	381	66	0.173
KSZ_03_3	0.398	0.015	0.053	0.002	0.161	333	10.0	340	9.9	350	110	539	476	0.883
KSZ_03_46	0.398	0.017	0.054	0.002	0.247	339	6.3	342	11	367	91	351	60	0.172
KSZ_03_12	0.399	0.016	0.054	0.002	0.268	337	10.0	340	11	390	100	730	95	0.131
KSZ_03_23	0.399	0.017	0.054	0.002	0.110	337	5.9	343	12	379	83	230	60	0.262
KSZ_03_73	0.492	0.023	0.060	0.002	0.568	378	7.6	406	15	585	77	864	19	0.022
KSZ_03_67	0.493	0.014	0.060	0.002	0.422	377	4.6	407	8.2	591	52	1320	187	0.142
KSZ_03_44	0.498	0.012	0.067	0.002	0.077	416	5.9	410	6.7	391	53	268	239	0.892
Discordant data														
KSZ_03_64	0.359	0.033	0.052	0.002	-0.014	328	9.5	309	24	300	190	356	131	0.368
KSZ_03_24	0.369	0.043	0.053	0.002	-0.161	333	9.1	313	31	230	230	375	217	0.578
KSZ_03_49	0.374	0.026	0.052	0.002	-0.073	327	7.3	320	18	260	150	539	81	0.151
KSZ_03_10	0.381	0.020	0.053	0.002	-0.057	335	6.0	326	14	270	110	1111	212	0.191
KSZ_03_55	0.384	0.014	0.052	0.001	-0.025	328	3.9	330	9.4	344	71	1191	274	0.230
KSZ_03_47	0.391	0.021	0.052	0.002	-0.110	328	6.9	336	15	390	120	624	101	0.163

APPENDIX 2 LA-ICP-MS U-Pb zircon data from exotic clasts from the Janoska stream, Outer Western Carpathians, SW-Poland

Sample ID	Final207_235 2 s		Final206_238 2 s		ErrorCorrelati	FinalAge206_ 2 s		FinalAge207_ 2s		FinalAge207_ 2s		U [ppm]	Th [ppm]	Th/U
Orthogneiss														
Variscan rims														
A1_16	0.403	0.023	0.0537	0.0013	0.0010	337	8.1	343	17	380	140	107	84	0.787
A1_27	0.433	0.016	0.0573	0.0025	0.2727	359	15	365	11	396	85	327	18	0.054
Cadomian rims														
A1_26	0.704	0.020	0.0885	0.0015	0.8489	547	8.6	541	12	535	48	730	10.0	0.014
A1_35	0.699	0.022	0.0852	0.0011	0.4205	527	6.8	538	13	594	63	624	1.5	0.002
Inherited cores														
A1_51	5.620	0.230	0.3420	0.0110	0.7332	1896	51	1917	35	1939	53	255	95	0.372
Discordant data														
A1_1	3.608	0.090	0.2634	0.0034	0.7842	1507	17	1550	20	1605	36	746	433	0.580
A1_2	3.127	0.053	0.2342	0.0038	0.7863	1356	20	1439	13	1555	26	143	41	0.285
A1_3	1.161	0.027	0.1056	0.0025	0.3926	647	15	782	13	1188	62	558	32	0.057
A1_4	2.692	0.089	0.1967	0.0037	0.5288	1158	20	1325	24	1575	37	786	243	0.309
A1_5	2.460	0.190	0.1810	0.0120	0.8456	1074	68	1255	54	1615	69	248	38	0.152
A1_6	4.015	0.075	0.2895	0.0043	0.7562	1639	21	1636	15	1647	25	153	49	0.319
A1_7	1.317	0.025	0.1113	0.0020	0.7368	680	12	856	11	1340	25	1037	106	0.103
A1_8	3.824	0.084	0.2748	0.0036	0.5063	1565	18	1596	18	1648	35	126	51	0.405
A1_9	3.340	0.032	0.2404	0.0021	0.7474	1389	11	1491	7.7	1631	13	1324	1219	0.921
A1_10	0.827	0.026	0.0931	0.0016	0.6095	574	9.3	611	15	723	56	785	9.6	0.012
A1_11	0.686	0.025	0.0785	0.0037	0.7114	487	22	530	15	756	80	680	36	0.053
A1_12	0.568	0.026	0.0725	0.0017	0.5892	451	10	456	16	488	77	444	2.5	0.006
A1_13	3.950	0.071	0.2849	0.0038	0.5803	1616	19	1623	15	1640	26	166	110	0.663
A1_14	3.978	0.080	0.2864	0.0043	0.4157	1623	22	1633	17	1641	36	88	49	0.561
A1_15	4.015	0.058	0.2880	0.0027	0.1203	1631	13	1637	12	1651	31	144	76	0.528
A1_17	3.301	0.045	0.2403	0.0022	0.5818	1388	11	1480	11	1613	20	790	0.6	0.001
A1_18	3.962	0.073	0.2869	0.0032	0.3689	1626	16	1628	16	1625	31	205	0.5	0.003
A1_19	3.958	0.071	0.2859	0.0036	0.4053	1621	18	1624	15	1645	31	156	0.5	0.003
A1_20	3.755	0.060	0.2721	0.0034	0.3696	1551	17	1583	13	1623	29	717	0.4	0.001
A1_21	3.706	0.037	0.2667	0.0019	0.6723	1524	9.6	1572	8.0	1640	14	2700	0.6	0.000
A1_22	3.688	0.044	0.2664	0.0024	0.2908	1523	12	1568	9.6	1642	24	280	0.4	0.001
A1_23	3.557	0.035	0.2611	0.0025	0.6783	1495	13	1540	7.9	1602	14	1886	0.6	0.000
A1_24	0.979	0.077	0.0845	0.0056	0.9626	522	33	684	39	1280	45	780	0.9	0.001
A1_25	3.612	0.057	0.2657	0.0037	0.6567	1519	19	1554	13	1617	22	1650	0.6	0.000
A1_28	2.537	0.087	0.1946	0.0042	0.5818	1146	22	1282	25	1484	49	191	0.5	0.003
A1_29	3.859	0.051	0.2836	0.0033	0.3689	1609	16	1605	11	1607	25	423	0.4	0.001
A1_30	3.809	0.093	0.2817	0.0034	0.4053	1600	17	1594	20	1586	49	97	0.4	0.004
A1_31	3.901	0.085	0.2854	0.0043	0.3696	1618	22	1613	18	1626	36	142	0.5	0.004
A1_32	2.559	0.065	0.1967	0.0042	0.6723	1158	23	1289	19	1533	49	350	0.4	0.001
A1_33	3.168	0.075	0.2371	0.0053	0.2908	1371	28	1453	19	1565	41	270	0.5	0.002
A1_34	2.957	0.066	0.2287	0.0030	0.6783	1328	16	1396	17	1517	30	409	0.6	0.001
A1_36	2.770	0.120	0.2066	0.0095	0.9491	1210	51	1346	33	1569	24	301	1.4	0.005
A1_37	0.819	0.022	0.0728	0.0014	0.6516	453	8.2	610	13	1219	42	708	0.3	0.000
A1_38	3.906	0.049	0.2778	0.0034	0.4045	1580	17	1615	10	1648	27	258	0.4	0.001
A1_39	3.962	0.072	0.2845	0.0042	0.5870	1614	21	1625	15	1652	28	130	0.5	0.004
A1_40	3.434	0.073	0.2515	0.0064	0.4970	1445	33	1511	17	1615	46	184	0.4	0.002
A1_41	4.030	0.100	0.2884	0.0035	0.4367	1633	17	1639	20	1648	44	145	0.5	0.003
A1_42	3.572	0.045	0.2630	0.0031	0.4618	1505	16	1543	10	1598	24	1490	0.4	0.000
A1_43	2.660	0.160	0.1980	0.0061	0.8023	1165	33	1316	42	1569	69	604	0.6	0.001
A1_44	3.560	0.130	0.2530	0.0092	0.8588	1453	48	1539	28	1618	39	431	0.7	0.002
A1_45	4.050	0.100	0.2832	0.0034	0.6415	1607	17	1643	21	1683	37	144	0.6	0.004
A1_46	3.560	0.033	0.2605	0.0018	0.7253	1492	9.3	1540	7.3	1616	14	2750	0.5	0.000
A1_47	3.903	0.058	0.2850	0.0034	0.4006	1616	17	1613	12	1616	28	122	0.4	0.004
A1_48	4.006	0.064	0.2879	0.0033	0.4202	1631	16	1635	13	1617	25	191	0.5	0.003
A1_49	4.003	0.093	0.2876	0.0029	0.4810	1629	15	1633	19	1627	37	106	0.5	0.005
A1_50	3.663	0.063	0.2692	0.0045	0.6035	1536	23	1562	14	1617	30	196	0.5	0.002
A1_52	3.600	0.160	0.2580	0.0110	0.8628	1476	56	1545	35	1655	32	368	1.1	0.003
A1_53	4.010	0.083	0.2917	0.0041	0.4297	1650	21	1635	17	1638	34	138	0.5	0.004
Discordia upper intercept age = 1635 ± 12 Ma; MSWD = 4.0														
Granite														
Variscan grains														
KSZ5_22	0.370	0.017	0.0518	0.0011	0.4302	325	6.9	320	15	241	9.0	243	110.7	0.456
KSZ5_72	0.374	0.017	0.0505	0.0015	0.5382	318	9.4	323	15	350	14	393	90.8	0.231
KSZ5_49	0.378	0.017	0.0512	0.0018	0.7215	322	11	326	15	358	12	720	241.0	0.335
KSZ5_39	0.382	0.016	0.0521	0.0011	0.4085	327	6.9	329	14	342	12	435	13.9	0.032
KSZ5_21	0.383	0.016	0.0516	0.0011	0.2524	324	6.9	329	14	342	13	413	71.6	0.173
KSZ5_40	0.386	0.015	0.0524	0.0010	0.4183	329	6.3	332	13	350	10	538	15.2	0.028

Concordia age = 325,7 ± 2,9; MSWD = 0,7; probability of concordance = 0,4														
Eo-Variscan and Caledonian zircon grains														
KSZ5_42	0.472	0.026	0.0583	0.0014	0.3162	365	8.8	393	22	537	27	130	85	0.657
KSZ5_45	0.477	0.023	0.0621	0.0028	0.4588	388	18	396	19	440	20	548	221	0.403
KSZ5_43	0.481	0.018	0.0642	0.0014	0.6121	401	8.7	399	15	379	11	352	47	0.134
KSZ5_41	0.485	0.018	0.0630	0.0015	0.5697	394	9.4	401	15	432	13	715	65	0.090
KSZ5_44	0.505	0.019	0.0656	0.0014	0.4424	410	8.7	415	16	440	14	382	33	0.085
KSZ5_61	0.519	0.024	0.0672	0.0032	0.8627	419	20	424	20	440	13	900	57	0.063
Meso- and Paleoproterozoic concordant zircon grains														
KSZ5_78	2.250	0.140	0.1983	0.0093	0.4819	1166	55	1197	74	1234	68	521	143	0.274
KSZ5_47	2.318	0.110	0.2046	0.0078	0.4775	1200	46	1218	58	1255	52	249	96	0.387
KSZ5_80	2.394	0.084	0.2116	0.0043	0.5931	1237	25	1241	44	1226	33	496	158	0.318
KSZ5_31	2.410	0.110	0.2128	0.0065	0.6790	1244	38	1246	57	1265	49	140	59	0.420
KSZ5_37	2.411	0.085	0.2102	0.0044	0.6007	1230	26	1246	44	1265	35	564	134	0.237
KSZ5_38	2.473	0.091	0.2175	0.0050	0.5764	1269	29	1264	47	1253	37	124	47	0.378
KSZ5_58	2.490	0.140	0.2130	0.0120	0.6551	1245	70	1269	71	1325	68	855	165	0.193
KSZ5_14	2.688	0.110	0.2248	0.0066	0.5897	1307	38	1325	54	1356	42	167	53	0.316
KSZ5_13	2.721	0.120	0.2324	0.0085	0.6184	1347	49	1334	59	1356	55	260	82	0.315
KSZ5_12	2.733	0.100	0.2315	0.0048	0.6742	1342	28	1337	49	1354	37	194	61	0.315
KSZ5_51	2.970	0.140	0.2340	0.0120	0.8093	1355	70	1400	66	1457	56	841	316	0.376
KSZ5_7	3.029	0.100	0.2437	0.0048	0.5499	1406	28	1415	47	1419	40	298	212	0.712
KSZ5_10	3.164	0.130	0.2504	0.0075	0.5647	1441	43	1448	60	1457	54	180	49	0.272
KSZ5_79	3.231	0.110	0.2531	0.0056	0.4890	1454	32	1465	50	1496	43	269	151	0.559
KSZ5_87	3.232	0.130	0.2528	0.0069	0.6263	1453	40	1465	59	1482	50	113	54	0.480
KSZ5_86	3.250	0.150	0.2548	0.0090	0.6932	1463	52	1469	68	1465	49	156	119	0.764
KSZ5_18	3.283	0.120	0.2571	0.0054	0.6263	1475	31	1477	54	1467	41	147	46	0.312
KSZ5_9	3.368	0.120	0.2595	0.0063	0.5922	1487	36	1497	53	1500	43	341	120	0.351
KSZ5_27	3.370	0.180	0.2600	0.0120	0.8632	1490	69	1497	80	1512	50	904	335	0.371
KSZ5_11	3.425	0.120	0.2614	0.0057	0.6817	1497	33	1510	53	1530	43	719	267	0.371
KSZ5_48	3.428	0.140	0.2588	0.0075	0.6717	1484	43	1511	62	1520	55	148	80	0.538
KSZ5_26	3.431	0.120	0.2656	0.0051	0.6454	1518	29	1512	53	1510	40	559	121	0.217
KSZ5_64	3.483	0.130	0.2570	0.0054	0.4320	1474	31	1523	57	1585	50	102	75	0.737
KSZ5_23	3.613	0.130	0.2743	0.0064	0.6946	1563	36	1552	56	1542	42	409	159	0.390
KSZ5_6	3.626	0.120	0.2752	0.0045	0.5299	1567	26	1555	51	1548	40	670	349	0.521
KSZ5_63	3.761	0.150	0.2787	0.0080	0.6724	1585	45	1584	63	1550	48	149	179	1.202
KSZ5_60	3.790	0.210	0.2770	0.0150	0.6565	1576	85	1591	88	1602	75	243	124	0.508
KSZ5_62	3.803	0.140	0.2807	0.0063	0.7302	1595	36	1593	59	1565	42	241	89	0.370
KSZ5_66	4.120	0.200	0.2931	0.0096	0.7418	1657	54	1658	80	1698	54	190	208	1.094
KSZ5_3	4.176	0.160	0.2924	0.0061	0.4819	1654	34	1669	64	1691	52	243	157	0.648
KSZ5_36	4.250	0.240	0.2800	0.0120	0.4549	1591	68	1684	95	1751	87	236	178	0.754
KSZ5_24	4.430	0.180	0.3062	0.0086	0.6882	1722	48	1718	70	1737	57	238	87	0.365
KSZ5_59	4.446	0.160	0.3048	0.0073	0.6651	1715	41	1721	62	1732	47	311	162	0.519
KSZ5_77	4.450	0.180	0.2990	0.0110	0.5857	1686	62	1722	70	1759	67	287	192	0.668
KSZ5_68	4.453	0.160	0.3071	0.0079	0.5927	1726	44	1722	62	1716	52	289	192	0.664
KSZ5_20	4.520	0.200	0.3020	0.0110	0.8612	1701	62	1735	77	1759	51	701	114	0.162
KSZ5_33	4.610	0.210	0.3130	0.0110	0.5859	1755	62	1751	80	1759	67	410	139	0.338
KSZ5_76	4.618	0.170	0.3102	0.0077	0.6935	1742	43	1753	65	1763	51	301	145	0.483
KSZ5_25	4.690	0.180	0.3210	0.0094	0.6494	1795	53	1765	68	1749	54	261	148	0.567
KSZ5_34	4.900	0.180	0.3141	0.0060	0.4975	1761	34	1802	66	1856	56	275	112	0.407
KSZ5_69	5.020	0.190	0.3272	0.0088	0.7379	1825	49	1823	69	1840	56	139	77	0.557
KSZ5_56	5.030	0.280	0.3172	0.0094	0.5472	1776	53	1824	102	1845	80	277	118	0.426
KSZ5_4	5.059	0.180	0.3260	0.0070	0.7085	1819	39	1829	65	1827	47	414	134	0.324
KSZ5_5	5.070	0.190	0.3231	0.0078	0.8092	1805	44	1831	69	1853	47	399	157	0.394
KSZ5_57	5.070	0.290	0.3280	0.0120	0.6037	1829	67	1831	105	1826	80	422	250	0.592
KSZ5_84	5.130	0.210	0.3240	0.0120	0.7495	1809	67	1841	75	1886	72	181	132	0.726
KSZ5_17	5.395	0.180	0.3375	0.0058	0.4280	1875	32	1884	63	1878	51	402	170	0.422
KSZ5_29	5.970	0.230	0.3587	0.0091	0.5917	1976	50	1971	76	1967	57	241	190	0.788
KSZ5_8	6.302	0.220	0.3659	0.0069	0.7179	2010	38	2019	70	2010	52	190	118	0.619
KSZ5_73	6.490	0.290	0.3722	0.0100	0.7246	2040	55	2045	91	2058	68	103	95	0.921
KSZ5_19	13.380	0.600	0.5140	0.0180	0.2159	2674	94	2707	121	2759	102	30	12	0.406
KSZ5_53	15.650	0.640	0.5510	0.0150	0.5500	2829	77	2856	117	2866	96	90	72	0.796
Discordant zircon grains														
KSZ5_65	3.705	0.140	0.2474	0.0074	0.5850	1425	43	1572	59	1813	64	694	539	0.777
KSZ5_2	3.084	0.120	0.2322	0.0054	0.6326	1346	31	1429	56	1540	43	1215	410	0.337
KSZ5_32	2.800	0.220	0.2005	0.0056	0.4891	1178	33	1356	107	1620	89	1447	536	0.370
KSZ5_54	0.560	0.038	0.0451	0.0010	0.2171	284	6.1	452	31	1419	89	388	161	0.415
KSZ5_70	0.710	0.051	0.0516	0.0026	0.6927	324	16	545	39	1559	74	1550	850	0.548
KSZ5_46	0.716	0.042	0.0634	0.0038	0.8719	396	24	548	32	1267	57	513	59	0.115
KSZ5_75	0.783	0.074	0.0553	0.0047	0.8134	347	29	587	55	1739	111	500	89	0.179

KSZ5_71	0.899	0.037	0.0947	0.0025	0.8426	583	15	651	27	896	25	942	92	0.098
KSZ5_67	1.091	0.046	0.0886	0.0028	0.8745	547	17	749	32	1389	38	1566	222	0.142
KSZ5_81	1.240	0.052	0.0758	0.0040	0.3922	471	25	819	34	1955	103	2890	226	0.078
KSZ5_85	1.242	0.048	0.0482	0.0013	0.6913	303	8.2	820	32	2719	81	2081	1802	0.866
KSZ5_82	1.572	0.090	0.1120	0.0048	0.7877	684	29	959	55	1659	60	4070	945	0.232
KSZ5_35	1.719	0.067	0.1307	0.0035	0.6430	792	21	1016	40	1526	50	540	149	0.276
KSZ5_16	2.350	0.120	0.2007	0.0058	0.6856	1179	34	1228	63	1318	48	271	119	0.437
KSZ5_50	2.370	0.240	0.1653	0.0094	0.8281	986	56	1234	125	1536	82	326	45	0.138
KSZ5_1	2.509	0.095	0.2079	0.0052	0.5673	1218	30	1275	48	1396	43	468	144	0.308
KSZ5_55	2.514	0.100	0.1973	0.0059	0.7749	1161	35	1276	51	1455	41	1175	465	0.396
KSZ5_74	4.030	0.210	0.2411	0.0100	0.6130	1392	58	1640	85	1949	86	1145	354	0.309
KSZ5_28	4.080	0.210	0.1853	0.0085	0.6888	1096	50	1650	85	2423	97	203	115	0.567
KSZ5_83	4.620	0.230	0.2667	0.0100	0.6238	1524	57	1753	87	2020	86	210	103	0.488
KSZ5_30	5.440	0.260	0.2980	0.0110	0.7643	1681	62	1891	90	2109	73	343	235	0.685
KSZ5_52	5.900	0.360	0.3220	0.0160	0.7710	1799	89	1961	120	2121	79	949	427	0.450
KSZ5_15	0.516	0.020	0.0422	0.0010	0.3889	266	6.3	422	16	1396	50	4550	1470	0.323
Paragneiss														
Neoproterozoic concordant grains/rims														
KSZ7_5	0.749	0.047	0.0921	0.0036	0.1452	568	22	568	36	611	39	81	32	0.392
KSZ7_25	0.757	0.034	0.0943	0.0022	0.2508	581	14	572	26	567	22	166	107	0.646
KSZ7_4	0.760	0.036	0.0949	0.0023	0.3458	584	14	574	27	571	25	55	25	0.448
KSZ7_2	0.765	0.033	0.0934	0.0038	0.7160	576	23	577	25	589	25	476	114	0.239
KSZ7_22	0.769	0.035	0.0945	0.0022	0.0999	582	14	579	26	571	26	102	42	0.413
KSZ7_39	0.775	0.032	0.0924	0.0021	0.3472	570	13	583	24	636	23	206	63	0.305
KSZ7_33	0.781	0.030	0.0951	0.0020	0.6379	586	12	586	23	596	17	523	174	0.333
KSZ7_6	0.783	0.040	0.0902	0.0033	0.3374	557	20	587	30	646	41	143	73	0.509
KSZ7_17	0.786	0.038	0.0980	0.0025	0.4253	603	15	589	28	537	21	87	63	0.729
KSZ7_31	0.787	0.040	0.0940	0.0036	0.3335	579	22	589	30	671	35	251	144	0.574
KSZ7_27	0.789	0.029	0.0966	0.0025	0.6265	594	15	591	22	593	18	429	186	0.434
KSZ7_34	0.791	0.033	0.0946	0.0026	0.4659	583	16	592	25	632	23	229	88	0.385
KSZ7_38	0.796	0.033	0.0956	0.0022	0.5233	589	14	595	25	625	21	214	82	0.385
KSZ7_24	0.800	0.032	0.0964	0.0024	0.4967	593	15	597	24	596	20	234	99	0.423
KSZ7_16	0.801	0.044	0.0964	0.0030	0.3735	593	18	597	33	629	33	82	48	0.587
KSZ7_36	0.801	0.045	0.0963	0.0037	0.5851	593	23	597	34	614	29	308	128	0.416
KSZ7_9	0.804	0.035	0.0983	0.0023	0.2432	604	14	599	26	589	24	157	77	0.488
KSZ7_28	0.807	0.037	0.0969	0.0026	0.4735	596	16	601	28	600	25	98	56	0.576
KSZ7_29	0.808	0.032	0.0982	0.0027	0.1998	604	17	601	24	622	26	172	102	0.593
KSZ7_21	0.810	0.046	0.0968	0.0041	0.7781	596	25	602	34	574	24	433	146	0.337
KSZ7_23	0.810	0.036	0.0955	0.0023	0.3508	588	14	602	27	646	24	113	50	0.440
KSZ7_41	0.811	0.032	0.0969	0.0021	0.4403	596	13	603	24	618	20	263	144	0.548
KSZ7_37	0.814	0.033	0.0968	0.0030	0.6174	596	18	605	25	625	22	317	69	0.216
KSZ7_10	0.817	0.034	0.1013	0.0030	0.1226	622	18	606	25	541	25	123	68	0.556
KSZ7_26	0.817	0.030	0.0988	0.0020	0.5976	607	12	606	22	611	18	690	358	0.519
KSZ7_12	0.822	0.030	0.0992	0.0021	0.5041	610	13	609	22	622	17	496	207	0.418
KSZ7_18	0.822	0.033	0.0997	0.0024	0.4758	613	15	609	24	604	20	149	124	0.833
KSZ7_11	0.825	0.037	0.1011	0.0026	0.3374	621	16	611	27	560	22	112	59	0.528
KSZ7_32	0.831	0.034	0.0976	0.0030	0.3403	600	18	614	25	657	29	332	116	0.349
KSZ7_3	0.834	0.041	0.0991	0.0036	0.4471	609	22	616	30	632	27	314	52	0.166
KSZ7_30	0.834	0.044	0.0980	0.0046	0.3743	603	28	616	32	742	37	189	99	0.525
KSZ7_19	0.846	0.033	0.0999	0.0031	0.5894	614	19	622	24	698	23	422	80	0.189
KSZ7_35	0.848	0.039	0.1008	0.0032	0.7041	619	20	624	29	614	22	505	171	0.339
KSZ7_1	0.907	0.034	0.1072	0.0019	0.4634	656	12	655	25	632	20	168	122	0.727
KSZ7_13	0.920	0.040	0.1095	0.0026	0.4662	670	16	662	29	625	24	210	42	0.201
KSZ7_14	0.935	0.042	0.1123	0.0039	0.4366	686	24	670	30	639	29	193	119	0.617
KSZ7_15	0.940	0.038	0.1104	0.0024	0.2355	675	15	673	27	660	24	147	101	0.687
Mesoproterozoic concordant core 1207,4 Ma ± 33,8														
KSZ7_8	2.297	0.110	0.2022	0.0071	0.8426	1187	42	1211	58	1250	43	506	141	0.278
Discordant grains.rims														
KSZ7_20	2.008	0.110	0.1701	0.0075	0.6503	1013	45	1118	61	1365	58	472	169	0.360
KSZ7_7	2.138	0.091	0.1870	0.0066	0.6971	1105	39	1161	49	1302	46	1609	430	0.270
KSZ7_40	2.138	0.086	0.1820	0.0051	0.5953	1078	30	1161	47	1327	44	2360	15	0.010
Granite														
Variscan rims														
KSZ8_15	0.375	0.017	0.0517	0.0014	0.6437	325	8.8	323	15	294	10	319	204	0.640
KSZ8_16	0.379	0.015	0.0523	0.0010	0.3065	329	6.3	326	13	333	13	199	159	0.801
KSZ8_51	0.385	0.015	0.0518	0.0010	0.4280	326	6.2	331	13	367	12	495	87	0.176
KSZ8_52	0.391	0.017	0.0530	0.0010	0.3211	333	6.3	335	15	375	14	315	314	0.997
KSZ8_17	0.393	0.021	0.0524	0.0018	0.4086	329	11	337	18	371	18	206	200	0.971
KSZ8_2	0.402	0.017	0.0550	0.0014	0.4950	345	8.8	343	15	350	12	373	49	0.131

Age = 330,6 ± 2,9 Ma MSWD = 0,36; probability of concordance = 0.55														
Neoproterozoic grains														
KSZ8_1	0.735	0.042	0.0884	0.0019	0.2097	546	12	559	32	636	34	178	86	0.485
KSZ8_28	0.743	0.045	0.0900	0.0034	0.3930	556	21	564	34	582	31	67	30	0.449
KSZ8_7	0.758	0.034	0.0923	0.0020	0.3020	569	12	573	26	589	24	110	27	0.242
KSZ8_19	0.759	0.029	0.0916	0.0026	0.4254	565	16	573	22	618	21	312	114	0.365
KSZ8_8	0.762	0.041	0.0911	0.0046	0.5928	562	28	575	31	636	27	876	26	0.030
KSZ8_4	0.764	0.031	0.0927	0.0020	0.4788	571	12	576	23	611	20	137	89	0.651
KSZ8_18	0.764	0.037	0.0917	0.0030	0.4506	566	19	576	28	636	24	746	28	0.038
KSZ8_32	0.765	0.030	0.0946	0.0025	0.3954	583	15	577	23	515	20	145	58	0.401
KSZ8_6	0.767	0.030	0.0950	0.0017	0.4874	585	10	578	23	563	17	298	195	0.654
KSZ8_26	0.768	0.032	0.0942	0.0023	0.5145	580	14	579	24	585	22	277	158	0.569
KSZ8_20	0.769	0.028	0.0936	0.0023	0.4592	577	14	579	21	545	19	419	270	0.644
KSZ8_42	0.769	0.031	0.0946	0.0025	0.3913	583	15	579	23	563	21	336	208	0.619
KSZ8_23	0.770	0.040	0.0927	0.0048	0.6332	571	30	580	30	589	26	790	84	0.106
KSZ8_27	0.770	0.039	0.0925	0.0029	0.4277	570	18	580	29	636	28	92	50	0.541
KSZ8_41	0.771	0.033	0.0939	0.0024	0.5790	579	15	580	25	582	21	112	36	0.324
KSZ8_43	0.772	0.043	0.0914	0.0035	0.4873	564	22	581	32	622	31	111	37	0.331
KSZ8_31	0.773	0.035	0.0921	0.0028	0.5188	568	17	581	26	625	24	134	54	0.399
KSZ8_24	0.774	0.041	0.0939	0.0057	0.7980	579	35	582	31	632	25	620	112	0.181
KSZ8_29	0.775	0.059	0.0902	0.0030	0.3684	557	19	583	44	646	42	58	27	0.464
KSZ8_14	0.776	0.028	0.0946	0.0021	0.3868	583	13	583	21	593	19	257	195	0.759
KSZ8_39	0.776	0.030	0.0929	0.0025	0.5271	573	15	583	23	632	21	729	328	0.450
KSZ8_5	0.777	0.037	0.0957	0.0032	0.5044	589	20	584	28	571	23	337	95	0.282
KSZ8_33	0.779	0.029	0.0958	0.0019	0.4151	590	12	585	22	593	19	442	255	0.577
KSZ8_10	0.780	0.032	0.0933	0.0027	0.5836	575	17	585	24	585	18	583	52	0.089
KSZ8_3	0.784	0.030	0.0944	0.0019	0.4045	582	12	588	22	622	20	500	224	0.448
KSZ8_40	0.785	0.029	0.0954	0.0026	0.4601	587	16	588	22	629	20	571	137	0.240
KSZ8_49	0.785	0.035	0.0956	0.0031	0.4701	589	19	588	26	578	21	306	85	0.278
KSZ8_48	0.787	0.036	0.0966	0.0036	0.5854	594	22	589	27	571	23	309	137	0.444
KSZ8_30	0.788	0.031	0.0941	0.0021	0.3907	580	13	590	23	625	22	349	118	0.339
KSZ8_44	0.791	0.037	0.0942	0.0034	0.4735	580	21	592	28	582	25	215	67	0.310
KSZ8_21	0.797	0.031	0.0954	0.0023	0.3712	587	14	595	23	629	25	708	18	0.025
KSZ8_9	0.800	0.033	0.0969	0.0032	0.6784	596	20	597	25	607	20	654	59	0.090
KSZ8_37	0.802	0.047	0.0954	0.0027	0.7885	587	17	598	35	636	22	412	35	0.084
KSZ8_54	0.804	0.032	0.0953	0.0022	0.3235	587	14	599	24	643	23	501	18	0.037
KSZ8_36	0.816	0.040	0.0954	0.0028	0.5214	587	17	606	30	722	32	505	66	0.131
KSZ8_25	1.165	0.073	0.1287	0.0059	0.5961	780	36	784	49	828	39	171	139	0.813
Mesoproterozoic cores														
KSZ8_47	2.345	0.093	0.2092	0.0063	0.6729	1225	37	1226	49	1204	40	364	135	0.372
KSZ8_50	2.405	0.110	0.2080	0.0140	0.5916	1218	82	1244	57	1345	94	274	49	0.179
KSZ8_45	2.535	0.130	0.2171	0.0094	0.6851	1267	55	1282	66	1336	51	218	115	0.526
KSZ8_12	3.430	0.350	0.2480	0.0190	0.8519	1428	109	1511	154	1609	88	536	99	0.185
KSZ8_55	4.210	0.200	0.2960	0.0130	0.6388	1671	73	1676	80	1672	70	235	73	0.310
Discordant grains/cores														
KSZ8_11	1.415	0.058	0.1127	0.0029	0.5080	688	18	895	37	1461	51	1330	244	0.183
KSZ8_13	0.875	0.035	0.0887	0.0027	0.5552	548	17	638	26	994	36	1395	220	0.158
KSZ8_22	0.863	0.059	0.0753	0.0033	0.3576	468	21	632	43	1260	75	2505	686	0.274
KSZ8_34	1.308	0.058	0.1226	0.0043	0.4964	746	26	849	38	1111	42	877	25	0.028
KSZ8_35	1.012	0.038	0.0323	0.0011	0.3476	205	7.0	710	27	3038	109	7930	5280	0.666
KSZ8_38	3.300	0.680	0.1880	0.0250	0.9618	1111	148	1481	305	1832	196	628	115	0.183
KSZ8_46	1.069	0.079	0.1018	0.0027	0.0759	625	17	738	55	1033	79	304	59	0.195
KSZ8_53	0.764	0.064	0.0839	0.0053	0.6415	519	33	576	48	778	42	460	47	0.102

APPENDIX 3 LA-ICP-MS U-Pb rutile data from A-2 sample, Janoska Stream, Outer Western Carpathians, SW-Poland												
sample No	207Pb/235U	2s	206Pb/238U	2s	R2	207Pb/206Pb	2s	R2	Pb/238U age [	2s	Pb/235U age [	2s
Concordant rutile												
A2RT_1	0.380	0.073	0.0569	0.0027	0.0881	0.0512	0.0095	0.1416	357	13	337	54
A2RT_2	0.443	0.086	0.0553	0.0029	0.0018	0.0610	0.0120	0.1991	346	15	349	62
A2RT_3	0.372	0.077	0.0536	0.0031	0.2168	0.0530	0.0110	0.1004	336	16	302	58
A2RT_4	0.398	0.017	0.0533	0.0016	0.1723	0.0538	0.0017	0.2248	335	3.9	340	9.3
A2RT_5	0.395	0.018	0.0540	0.0017	0.1944	0.0538	0.0018	0.2110	339	5.0	337	10
A2RT_6	0.399	0.021	0.0555	0.0018	0.1905	0.0524	0.0026	0.1580	348	5.5	340	13
A2RT_8	0.364	0.035	0.0542	0.0023	0.0929	0.0481	0.0051	0.2601	340	10	317	26
A2RT_9	0.405	0.033	0.0530	0.0021	0.1802	0.0544	0.0044	0.2937	333	8.8	341	23
A2RT_10	0.367	0.046	0.0559	0.0021	0.0158	0.0493	0.0060	0.2224	351	8.7	321	35
A2RT_11	0.444	0.064	0.0552	0.0022	-0.1292	0.0606	0.0088	0.3027	346	9.7	364	43
A2RT_12	0.428	0.059	0.0574	0.0027	-0.0368	0.0546	0.0074	0.3634	360	13	354	40
A2RT_14	0.400	0.036	0.0544	0.0021	-0.2671	0.0533	0.0053	0.5094	342	9.0	339	25
A2RT_15	0.389	0.041	0.0544	0.0022	0.0542	0.0528	0.0056	0.2580	341	9.5	335	30
A2RT_16	0.405	0.038	0.0548	0.0020	0.0978	0.0541	0.0050	0.1686	344	8.1	344	25
A2RT_17	0.425	0.047	0.0551	0.0022	0.1380	0.0570	0.0061	0.1332	347	9.7	351	32
A2RT_19	0.384	0.053	0.0556	0.0027	-0.2385	0.0515	0.0075	0.4763	349	13	329	37
A2RT_20	0.396	0.015	0.0563	0.0018	0.1112	0.0522	0.0015	0.3600	353	5.0	340	7.4
A2RT_22	0.400	0.021	0.0551	0.0019	0.1471	0.0521	0.0025	0.2983	346	7.0	340	13
A2RT_23	0.394	0.027	0.0554	0.0019	0.0674	0.0520	0.0033	0.1930	347	6.6	335	18
A2RT_24	0.373	0.054	0.0554	0.0025	0.0918	0.0491	0.0069	0.2254	348	12	338	37
A2RT_25	0.423	0.020	0.0560	0.0018	0.1204	0.0546	0.0024	0.2849	351	5.5	359	11
A2RT_26	0.413	0.029	0.0571	0.0021	0.0683	0.0524	0.0036	0.3270	358	8.2	350	19
Concordia age = 344.7 ± 2.5; MSWD = 2.5; probability of concordance = 0.11												
A2RT_27	0.485	0.046	0.0663	0.0031	0.1848	0.0531	0.0046	0.1511	414	15	399	29
Discordant rutile												
A2RT_21	0.482	0.079	0.0556	0.0028	-0.0989	0.0580	0.0100	0.3038	351	15	385	53
A2RT_18	0.510	0.120	0.0581	0.0036	0.2074	0.0630	0.0150	-0.0795	363	20	383	78
A2RT_7	0.741	0.076	0.0583	0.0030	0.3709	0.0888	0.0070	0.0135	365	15	559	41
A2RT_13	0.795	0.085	0.0566	0.0025	-0.1272	0.1030	0.0120	0.4402	355	12	595	47